

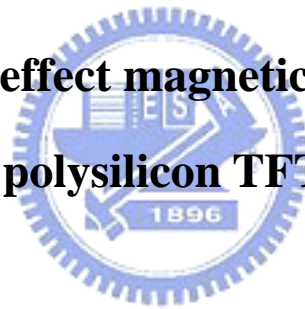
國立交通大學

電子工程學系電子研究所碩士班

碩士論文

薄膜電晶體磁場感測器之研究

**A study of Hall effect magnetic sensors based on
polysilicon TFTs**



研究生：蕭宇盛

指導教授：張國明 博士

中華民國九十四年六月

薄膜電晶體磁場感測器之研究

**A study of Hall effect magnetic sensors based on
polysilicon TFTs**

研究生：蕭宇盛

Student : Yu-sheng Xiao

指導教授：張國明 博士

Advisor : Dr. Kow-Ming Chang

國立交通大學電子工程學系電子研究所碩士班



Submitted to Institute of Electronics
College of Electrical Engineering and Computer Science
National Chiao Tung University
In Partial Fulfillment of the Requirements
for the Degree of
Master of Science
In
Electronics Engineering

June 2005
Hsinchu, Taiwan, Republic of China

中華民國九十四年六月

薄膜電晶體磁場感測器之研究

研究生：蕭宇盛

指導教授：張國明 博士

國立交通大學

電子工程學系 電子研究所碩士班

摘要



現今的薄膜電晶體(TFT)已經發展許多年，製程技術可以說相當成熟，由於使用成本低廉的玻璃基板加上低溫製程的技術，因此目前薄膜電晶體被廣泛的應用於液晶螢幕的開關。然而，從近一、兩年的國外研究報告來看，許多薄膜電晶體的感測應用逐漸浮出檯面，甚至有些薄膜電晶體的感測器已經有商業產品。本篇論文中，我們將利用薄膜電晶體結合磁場感測原理來實現霍爾效應感測器(Hall effect sensor)。整個元件製程溫度跟一般薄膜電晶體依樣都控制在 600 度以下。此外，我們將針對不同幾何結構的薄膜電晶體來分析各種感測元件的霍爾電壓(Hall voltage)模態，對於不同結構所得到的霍爾電壓(Hall voltage)、電壓偏移(offset)也將做一個深入的探討。藉由各種不同結構元件的設計、製作、量測到分析，我們可以獲得最佳化的磁場感測元件。

A study of Hall effect magnetic sensors based on polysilicon TFTs

Student : Yu-sheng Xiao

Advisor :Kow-Ming Chang

Department of Electronics Engineering

and Institute of Electronics

National Chiao Tung University



Abstract

Nowadays TFT has developed for many years, and its fabricating technic is very mature. Due to using low-cost glass substrate and low-temperature fabrication technology, TFT has widespread application to use in switching devices of LCD. However, from the latest foreign research reports, many applications of TFT has emerged, and some commercial products of TFT application has appeared. In this thesis, we will develop a new Hall Effect sensor by using thin film transistor integrated with magnetic sensing principle. In the whole device fabrication, the processing temperature is been controlled below 600 degrees as well as other conventional TFT. In addition, we will analyze Hall voltage mode of magnetic

sensors by use of various geometries of TFT. We also do a intensive discussion about Hall voltage and Bias offset due to different structures. By way of various geometry designs, device fabrication, characteristic measurement, we will be able to obtain optimal magnetic sensing devices.



誌謝

首先非常感謝我的指導教授張國明博士，老師亦師亦友的指導方式讓我獲益匪淺，讓我體會到做研究應有的態度，謝謝老師。

感謝林林稔杰學長細心指導，好幾次熬夜到天亮陪我做量測，也適時給我明確的方向，使我得到許多不一樣的經驗與啟發。同時要感謝黃士軒、謝孟帆、沈志浩同學，大夥一起做實驗、畫圖，共同渡過最艱辛的一段，讓我的實驗能順利完成。假如沒有你們跟我一起並肩努力，我的研究過程將是寂寞黯淡的。

謝謝交通大學提供了非常完善的實驗設備，讓我的實驗可以順利完成，還要感謝技術員的幫忙，實驗期間機台時常發生故障，還好有技術員全力搶修，讓大家的實驗得以持續進行。

謝謝在交大陪我走過風風雨雨的同學、學長以及我的好朋友們，因為有大家的陪伴，互相激勵、互相協助，才能順利取得學位，謝謝大家。

最後我要將這篇論文獻給我的父母，蕭尚林先生與蔡春桂女士。感謝他們從小到大對我的栽培跟養育，讓我在沒有後顧之憂之下可以順利完成學業，爹、娘，謝謝你們，我愛你們。

Contents

ABSTRACT (in Chinese).....	i
ABSTRACT (in English).....	ii
ACKNOWLEDGEMENTS.....	iv
CONTENTS.....	v
FIGURE CAPTIONS.....	vii
Chapter 1 Introduction	1
1.1 The Development of Magnetic Field Sensors.....	1
1.2 TFT Magnetic-Field Sensors.....	2
1.3 Applications.....	3
Reference.....	5
Chapter 2 Theory	7
2.1 The Hall Effect.....	7
2.2 Hall Effect in semiconductor.....	9
2.3 Recrystallization of Amorphous Si (a-Si) Thin Films.....	10
2.3.1 Solid Phase Crystallization.....	10
2.3.2 Excimer Laser Annealing Crystallization.....	11
2.3.3 Metal-Induced Lateral Crystallization.....	11
2.4 The Geometrical Correction Factor.....	11
2.5 Basic characteristics.....	13
2.6 Structure design.....	14
Reference.....	16
Chapter 3 Experimental Procedure	17
3.1 The Fabrication Process Flow.....	17
3.2 Measurements.....	19

3.2.1 Electronic Bench Equipment.....	19
3.2.2 Magnetic Instrumentation.....	19
Reference.....	21
Chapter 4 Results and Discussion	22
4.1 Transistors Characteristics.....	22
4.1.1 The Output Characteristics of Our Proposed Magnetic Sensor.....	22
4.1.2 The transfer characteristics of our proposed magnetic sensor.....	22
4.2 Sensors Characteristics.....	23
4.2.1 The Comparison of The Hall Voltage Versus V_{ds}	23
4.2.2 The Voltage of Sensing Electrode Pad Varies with Time.....	24
4.2.3 The Offset Voltage V_{off}	25
Reference.....	27
Chapter 5 Conclusions and future work	28
5.1 Conclusion.....	28
5.2 Future work.....	28
References.....	30



Figure Captions

Chapter 2

Fig. 2-1 The schema of the Hall effect in bulk	31
Fig. 2-2 the profile structure of Hall sensor	31
Fig. 2-3 the different electrode designs of structure	32

Chapter 3

Fig. 3-1 Process flow of fabricating proposed magnetic field sensor	35
Fig. 3-2 Profile schematic of the Hall sensor	37
Fig. 3-3 The schematic of the measurement	38
Fig. 3-4 The schematic of applied voltage	38

Chapter 4

Fig. 4-1 I_{ds} - V_{ds} output characteristics of our proposed magnetic sensor based on TFT structure with versus V_{gs} ; $W/L = 80 \mu m/150 \mu m$; sensing pad is closed to source with the $35 \mu m$	39
Fig. 4-2 I_{ds} - V_{gs} transfer characteristics of our proposed magnetic sensor based on TFT structure for $V_{ds} = 5, 10, 15, 20, 25 V$; $W/L = 80 \mu m/150 \mu m$; sensing pad is closed to source with the $35 \mu m$	39
Fig. 4-3 Comparison of the Hall voltage versus V_{ds} for $V_{gs} = 10, 15, 20, 25, 30 V$; $W/L = 80 \mu m/150 \mu m$; sensing pad is closed to source with the $35 \mu m$	40
Fig. 4-4 The voltage of sensing electrode pad varies with time with/without magnetic field bias and Hall voltage versus time for $V_{gs} = 15V$, $V_{ds} = 3.5V$; $W/L = 80 \mu m/150 \mu m$; sensing pad is closed to source with the $35 \mu m$	41
Fig. 4-5 The voltage of sensing electrode pad varies with time with/without magnetic field bias and Hall voltage versus time $V_{gs} = 20V$, $V_{ds} = 7.5V$; $W/L = 80 \mu m/150 \mu m$; sensing pad is closed to source with the $35 \mu m$	41
Fig. 4-6 Comparison of the Hall voltage versus V_{ds} for $V_{gs} = 15, 20, 25, 30 V$; $W/L = 80 \mu m/150 \mu m$; sensing pad is closed to drain with	

the 35 μ m	42
Fig. 4-7 The voltage of sensing electrode pad varies with time with/without magnetic field bias and Hall voltage versus time for $V_{gs} = 25V$, $V_{ds} = 15V$; $W/L = 80 \mu m/150 \mu m$; sensing pad is closed to drain with the 35 μ m	43
Fig. 4-8 I_{ds} - V_{ds} output characteristics of our proposed magnetic sensor based on TFT structure with versus V_{gs} ; $W/L = 40 \mu m/100 \mu m$; sensing pad is closed to source with the 20 μ m	44
Fig. 4-9 I_{ds} - V_{gs} transfer characteristics of our proposed magnetic sensor based on TFT structure for $V_{ds} = 2,6,10,14,18 V$; $W/L = 40 \mu m/100 \mu m$; sensing pad is closed to source with the 20 μ m	44
Fig. 4-10 Comparison of the Hall voltage versus V_{ds} for $V_{gs} = 10,15,20,25,30 V$; $W/L = 40 \mu m/100 \mu m$; sensing pad is closed to source with the 20 μ m	45
Fig. 4-11 The voltage of sensing electrode pad varies with time with/without magnetic field bias and Hall voltage versus time for $V_{gs} = 25V$, $V_{ds} = 20V$; $W/L = 40 \mu m/100 \mu m$; sensing pad is closed to source with the 20 μ m	46
Fig. 4-12 I_{ds} - V_{ds} output characteristics of device 1 versus V_{gs} ; $W/L = 40m/100m$; sensing pad is closed to drain with the 20m	47
Fig. 4-13 I_{ds} - V_{ds} output characteristics of device3 versus V_{gs} ; $W/L = 40m/100m$; sensing pad is closed to drain with the 20m	47
Fig. 4-14 Comparison of the Hall voltage versus V_{ds} for $V_{gs} = 10,15,20,25,30 V$; $W/L = 40 \mu m/100 \mu m$; sensing pad is closed to drain with the 20 μ m; S1 is one of the sensing pads	48
Fig. 4-15 The voltage difference of sensing electrode pad varies with time with/without magnetic field bias and Hall voltage versus V_{ds} for $V_{gs} = 10,15,20,25,30 V$; $W/L = 40 \mu m/100 \mu m$; sensing pad is closed to drain with the 20 μ m	49
Fig. 4-16 The partial region of the Fig. 4-16	49
Fig. 4-17 Comparison of the Hall voltage versus V_{ds} for $V_{gs} = 10,15,20,25,30 V$; $W/L = 40 \mu m/100 \mu m$; sensing pad is closed to drain with the 20 μ m; S2 is another pad	50
Fig. 4-18 Comparison of the offset voltage versus V_{ds} for $V_{gs} = 10,15,20,25,30 V$; $W/L = 40 \mu m/100 \mu m$; sensing pad is closed to drain with the 20 μ m	51
Fig. 4-19 The voltage gap between two pads with magnetic field versus V_{ds} for $V_{gs} = 10,15,20,25,30 V$; $W/L = 40 \mu m/100 \mu m$; sensing	

pad is closed to drain with the $20\ \mu$

51



Chapter 1

Introduction

1.1 The Development of Magnetic Field Sensors

Semiconductor magnetometers provide an excellent means of measuring both magnetic field intensity and direction. Fast response, high sensitivity, good reliability are advantages over other conventional magnetometer alternatives. Even more, the semiconductor magnetometers are small size, low cost and can be combined with the semiconductor integration circuits. It makes possible to transfer magnetic signal into electrical signal, which can be operated as some useful function. With extremely low magnetic field sensitivity capability and a user configurable command set, the TFT (Thin Film Transistor) magnetometers fabrication technology is the most important technique index to solve a variety of problems in custom applications [1]-[4]. Possible magnetometer applications include process control, anomaly detection, laboratory instrumentation, traffic and vehicle detection, security systems, compassing, magnetic ink recognition, current sensing, and space motion detection [5]. Our extensive experiments in fabricating magneto sensor devices allow us to develop electronic compass modules that are suited to the earth's crust, the atmospheric layer and the oceanic trench.

Magnetic field sensors, magnetic switches and instruments measure magnetic fields and/or magnetic flux by evaluating a potential (Hall effect), current (wire coil / flux gate), or resistance change because of the field strength and direction. They are used to study the magnetic field or flux around permanent magnets, coils, and electrical devices. TFT magnetic field sensor devices are semiconductor devices in which the electrical voltage drop is a function of the environmental magnetic field [6]. Magnetic flux induces the electron charges accumulated in the sensing electrode pads and perform a continuous measurement of the voltage differences in the magnetic field at the ends of the sensing electrode pads. Hall effect describes a device that converts the energy stored in a magnetic field to an electrical signal by means of the development of a voltage between the two sensing electrode pads of current TFT

devices which can be applied in any particular environments to measure the magnetic field.

Flux density, measured in Tesla or Gauss, is the most important specification to be considered when selecting between the available magnetic field sensors and magnetic switches. Numbers of axes of measurement is also important. Some of these instruments also measure the direction of the magnetic field, including bipolar measurements. They can also measure how large the magnetic field is. Accuracy is represented as a percentage of full scale. Resolution represents the smallest change in reading the sensor can detect. Sensitivity (V/Tesla or V/Gauss) is the most important factor to consider as well.

Outputs for magnetic field sensors, magnetic switches and instruments can be analog current, voltage or frequency; digital, such as TTL; or computer signals, parallel or serial signals being the most common [7]. These devices can also be switches or alarms. They can be sensor elements, sensors with some built-in signal conditioning, and gauges with no output or as sophisticated as an instrument with a video display and many outputs. They can also be the totalizers and the data recorders.

1.2 TFT Magnetic-Field Sensors

Nowadays, Magnetometer is widely applied to MRAM、OSD (Optical-super-density)、many kinds of sensors. Magnetic field sensor is superior to optical position sensor because the optical film is easy polluted on the worst environment. Fabrication technology of thin film transistor is very mature in Taiwan. The cost of thin film transistor is gradually decreased due to bulk production of TFT (Thin Film Transistor). Fabrication technology is so mature that it could enlarge its applications to all kinds of family electrical applications. Generally, as the higher mobility in the channel, the thinner of the channel, and the lower concentration in the channel under gate voltage bias, the device has better performance in measuring the magnetic field. The major substrate material is silicon for the magnetic sensor because silicon-manufacturing technology is very mature and reliable. Besides, the sensing devices, the signal processors, and drive circuits are made on one chip

simultaneously with silicon compatible process can achieve the smart sensor. This method can reduce external environmental noise and the cost of the device fabrication; on the other hand, it also can add sensitivity of the sensor. A large number of magnetometers are made with similar MOSFET structure having higher temperature process, but this structure is not suitable for glass or flexible substrates [8], [9]. In addition, magnetic sensing sensitivity of silicon substrate is easy to be interfered with the magnetic field. These problems can be avoided by using glass substrates.

A list of criteria for magnetic field sensor design comprises the following items [10] :

- compatibility with microelectronics technologies
- design of the device
- output signal : voltage or current
- manufacturing cost
- device geometry
- sensitivity
- the ratio of signal and noise
- time resolution
- linearity
- temperature coefficient of sensitivity
- offset
- power consumption, size
- electrical input and output impedance
- stability, reliability, lifetime



1.3 Applications

Consider a Hall effect sensor : the primary quantity measured is the component of magnetic induction perpendicular to the plane of the sensor, averaged over the active area, An example of a primary application of this world be a Hall effect Gaussmeter. At the secondary level a Hall sensor can be used in a proximity switch, wherer it is acting as a position sensor by virtue of the spatial variation of magnetic induction near a permanent magnet. Sensors are used in applications covering almost

every area of human activity. It is helpful to classify these areas, because the priorities vary widely from one to another. Areas of application for sensors is listed as follows [11] :

- Aerospace
- Automotive
- Biomedical
- Consumer/domestic
- Industrial : Chemical/Construction/Electrical/Mechanical
- Scientific research
- Surveying and prospecting

Furthermore, the thin film transistor on glass substrate accompany with the lower leakage current, the lower power consumption and the higher on-off current ratio compare to the MOSFET on silicon substrate. These advantages will promote the performance widely in the fabrication of the magnetic sensor array lately. As the foreign scientific or technical literature reported, only several few research papers mentioned the fabrication of the magnetic sensor using the thin film transistor structure. According to these literatures, we find that these devices are not the real thin film transistors, the improper device's architecture design and without suitable fabrication flow, lead to the bad performance in these sensor devices. Consequently, our research project design a series experiments to develop the complete technology of TFT magnetic sensor device, for measuring and analyzing the magnetic field distribution of direction and density in the space. We design several kinds of geometric structures TFT magnetic sensor with different dimensions to realize and analyze the effects of the magnetic sensitivity, Hall voltage, and the signal to noise ratio on the TFT magnetic sensor. Thanks to the mature technology in TFT process, high yield and stability produced, we can integrate the sensor devices with sensor circuits in unit process flow. By means of parallel array sensor devices, it will increase the magnetic sensitivity, decrease the disturbance of environment noises and enhance the sensing analyzability.

Reference

- [1] L. Dong, R.F. Yue, “A high performance single chip uncooled a-Si TFT infrared sensor”, Solid-State Sensors, Actuators and Microsystems, 12th International Conference, Vol.1, pp.312 – 315, 2003.
- [2] Hara, H.; Sakurai, M,” Low temperature polycrystalline silicon TFT fingerprint sensor with integrated comparator circuit”, Proceeding of the 30th European, 21-23 Sept. 2004
- [3] Hashido, R.; Suzuki, A.” A capacitive fingerprint sensor chip using low-temperature poly-Si TFTs on a glass substrate and a novel and unique sensing method”, Solid-State Circuits, IEEE Journal of , Volume: 38 , Issue: 2 , Feb. 2003
- [4] Carvou, E.; Le Bihan, F, “Hall effect magnetic sensors based on polysilicon TFTs”,
Sensors Journal, IEEE, Volume: 4 , Issue: 5, pp.597 – 602, 2004.
- [5] Rouse, G.; French, H.; Sasaki, H.; Kawai, T. “A solid-state vehicle detector for roadway applications”Vehicle Navigation and Information Systems Conference, 1995. Proceedings. In conjunction with the Pacific Rim TransTech Conference. 6th International VNIS. 'A Ride into the Future' 30 July-2 Aug. 1995 Page(s):11 – 16
- [6] Carvou, E.; Le Bihan, F.; Rogel, R.; Bonnaud, O. “Magnetic sensors with polysilicon TFTs” Sensors, 2002. Proceedings of IEEE, Volume 2, 12-14 June 2002 Page(s):804 - 809 vol.2
- [7] Kaulberg, T.; Bogason, G.” Am angledetector based on magnetic sensing” Circuits and Systems, 1994. ISCAS '94., 1994 IEEE International Symposium on Volume 5, 30 May-2 June 1994 Page(s):329 - 332 vol.5
- [8] Rodriguez-Torres, R.; Gutierrez-Dominguez, E.A, “Analysis of split-drain MAGFETs”, Electron Devices, IEEE Transactions, Vol. 51, Issue 12, pp.2237~ 2245, 2004.
- [9] Doyle, J, “High sensitivity silicon magnetic field detector”, Custom Integrated Circuits, IEEE Conference, pp.105 – 108, 2001

- [10] Henry D. Baltes and Radivoje S. Popovic, Integrated Semiconductor MagneticField Sensors, Proceedings of the IEEE, vol.74, No.8, pp.1107, 1986
- [11] Gopel, W. & Hesse, J. & Zemel, J. N. ed. "Sensors : a comprehensive survey : magnetic sensors"New York/VCH/c1989



Chapter 2

Theory

2.1 The Hall Effect

The Hall Effect is a physical effect arising in matter carrying electric field in the presence of a magnetic field. Fig. 2-1 shows bulk materials with free electron carriers under the applied voltage. Suppose that in this bulk material, along the +x direction, an external electric field E_e is established. Then we applied a uniform magnetic field in the +z direction. From Lorentz force we know that the electrons will be affected by the magnetic field. Electrons will be pushed towards +Y direction. The interaction is described by the Lorentz force :

$$F = q(v \times B) \quad (2.1)$$

Where F is the Lorentz force expressed by a charge carrier of charge moving with velocity v in a magnetic flux density B . The force F pushes carriers toward the back side of the bulk. Consequently the carrier concentration at the back side of the bulk starts to increase, while the carrier concentration at the front of the bulk starts to decrease. Then an electric field E_H appears between the two edges. This field, E_H acts on the moving carriers too, and the transverse electrical force becomes strong enough to balance the magnetic force eventually. The transverse electric field E_H is called the Hall electric field. In this balance condition, we can get this equation:

$$q_0 E_H + q_0 * v \times B = 0 \quad (2.2)$$

and

$$E_H = -v \times B \quad (2.3)$$

This means that the Hall field is a function of the velocity of the carriers and the strength of the magnetic field. For a transducer with a given width W between sense electrodes, the Hall electric field can be integrated over W , assuming it is uniform, then

$$V_H = -WvB \quad (2.4)$$

Therefore, the Hall voltage is a linear function of :

- (a) The carrier velocity in the body of the transducer
- (b) The applied magnetic field in the sensitive axis
- (c) The spatial separation of the sense contacts

Consider the case of a piece of conductive material with a given cross section area of “A”. The carrier drift velocity can be determined by :

$$v = \frac{I}{q_0 * N * A} \quad (2.5)$$

where v is carrier velocity, I is current, q_0 is the charge on an electron, N is the carrier density, A is the cross section area.

So we can derive an expression that describes sensitivity of a Hall transducer as a function of cross sectional dimensions, current, and carrier density.

$$V_H = \frac{I * B}{q_0 * N * d} \quad (2.6)$$

Where d is the thickness of the conductor.

Besides, the resistance of the Hall transducer is a function of the conductivity and the geometry, for a rectangular slab, the resistance can be calculated by :

$$R = \frac{\rho * l}{w * d} \quad (2.7)$$

Where R is resistance, ρ is the resistivity, l is the length, w is the width, and d is the thickness. We suppose that the magnetic field is constant. From equation 2.1, if we want higher hall voltage, we must select higher biased current, material of lower implanted concentration and of thinner thickness. But higher biased current will cause higher consumption of the power and instable characteristic of device. From equation 2.2, material of lower implanted concentration and thinner thickness will cause higher resistance of material.

From equation 2.6 and 2.7, there is no sufficient information to select appropriate material and design structure of device. In our study, we employ traditional thin film transistor to carry out the hall sensor. We use inversion layer of MOS as sensing region and has to analyze the basic sensing mode of sensing region. In general, hall effect sensor has two sensing modes which we can measure the hall

voltage to compute the intensity of magnetic field for longer structure of device and employ Lorentz current to compute the intensity of magnetic field for wider structure of device. The followings we specifically make a sample analysis from two different modes to obtain what information we need to design the structure of device.

2.2 Hall Effect in semiconductor

In n-type semiconductor materials, we can derive a equation when there is no magnetic field applied to the semiconductor :

$$J_n(0) = \sigma_n \varepsilon + qD_n \nabla n \quad (2.8)$$

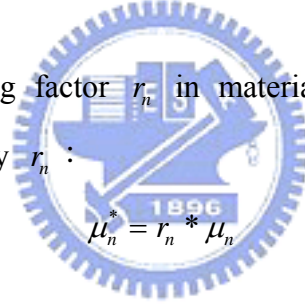
where σ_n is conductivity, D_n is diffusion coefficient, n is carrier concentration.

When a magnetic field is applied to semiconductor materials, the current density can be described by the equation :

$$J_n(B) \approx [J_n(0) + \mu_n B \times J_n(0) + \mu_n^2 B \bullet J_n(0)B][1 + (\mu_n B)^2]^{-1} \quad (2.9)$$

where μ_n is drift mobility

If we consider the scattering factor r_n in materials, we will substitute Hall mobility μ_n^* for drift mobility μ_n :



$$\mu_n^* = r_n * \mu_n \quad (2.10)$$

Then, we can get:

$$J_n(B) = [J_n(0) + \mu_n^* B \times J_n(0) + K(\mu_n^*)^2 B \bullet J_n(0)B][1 + (\mu_n^* B)^2]^{-1} \quad (2.11)$$

If we neglect the carrier concentration gradient, we will simplify the equation :

$$J_n(B) = \sigma_{nB} [\varepsilon + \mu_n^* B \times \varepsilon + K(\mu_n^*)^2 (B \bullet \varepsilon)B] \quad (2.12)$$

$$\sigma_{nB} = \sigma_n [1 + (\mu_n^* B)^2]^{-1}$$

Lorentz force produced by the vertical electric field, and the vertical field is produced by our proposed Hall sensor using external magnetic field and itself electric field.

Thus, we can get :

$$J_{nx} = \sigma_{nB} (\varepsilon_x - \mu_n^* B \varepsilon_y) \quad \text{and} \quad J_{ny} = \sigma_{nB} (\varepsilon_y + \mu_n^* B \varepsilon_x) \quad (2.13)$$

Now we consider the Hall voltage mode of operation, let us consider the long and thin sample, and there is no current in y direction, $J_{ny} = 0$

$$J_{ny} = \sigma_{nB} (\varepsilon_y + \mu_n^* B \varepsilon_x) = 0 \quad , \quad \varepsilon_y + \mu_n^* B \varepsilon_x = 0 \quad (2.14)$$

$$\rightarrow \varepsilon_y = -\mu_n^* B \varepsilon_x = R_H J_{nx} B \quad (2.15)$$

$$\text{where } R_H : \text{Hall coefficient} = -\frac{\mu_n^*}{\sigma_n} = -\frac{r_n}{qn} \quad (2.16)$$

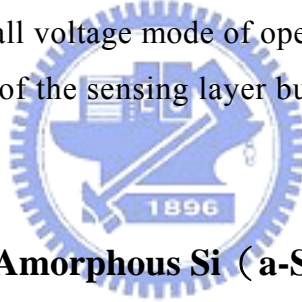
$$\text{and define a angle } \theta_H, \tan \theta_H = \frac{\varepsilon_y}{\varepsilon_x} = -\mu_n^* B = \sigma_n R_H B \quad (2.17)$$

The Hall coefficient is the proportionality factor relating the Hall field or the Hall voltage to the current-magnetic field product in a Hall effect experiment. The value and stability of the Hall coefficient directly determines the magnitudes and the stability of the sensitivity of the sensors based on the Hall effect.

For a sensing layer with thickness t , we can derive the Hall voltage and relative sensitivity

$$V_H = \frac{R_H IB}{t}, \quad \frac{V_H}{IB} = \frac{R_H}{t} = -\frac{r_n}{qnt} \quad (2.18)$$

Thus, we can find that the Hall voltage mode of operation is dependent of carrier concentration and thickness of the sensing layer but independent of carrier Hall mobility [1].



2.3 Recrystallization of Amorphous Si (a-Si) Thin Films

Generally, as the higher mobility in the channel, the thinner of the channel, and the lower concentration in the channel under gate voltage bias, the device has better performance in measuring the magnetic field. For LTPS TFTs, there are three kinds of low temperature crystallization methods and they are roughly reviewed.

2.3.1 Solid Phase Crystallization

Amorphous silicon thin films deposited by low-pressure chemical vapor deposition (LPCVD) below 600°C annealed in furnace at 600°C several hours (~ 24 h). The films will be converted into polycrystalline form, and the grain sizes obtained by this method (SPC) is more larger and smoother morphology than as-deposited poly-Si films. However, due to the low deposition temperature used, long crystallization duration is necessary, and large defect density exists in crystallized poly-Si.

2.3.2 Excimer Laser Annealing Crystallization

Laser crystallization is a much faster process than others. Especially, excimer laser crystallization is by far most widely used method now [2]-[4]. Because excimer laser is the strong absorption of UV light in silicon, most of the laser energy is deposited close to the surface of the a-Si films. The laser process heats the a-Si films to the melting point in a very short duration (several nanoseconds) without damaging the glass substrate, and the silicon films will melt and recrystallize. Because ELA process has the highest annealing temperature among the other methods, we can obtain the higher quality poly-Si films.

2.3.3 Metal-Induced Lateral Crystallization

A certain metal, for example, Al [5], Cu [6], Ag [7], or Ni [8], are deposited on a-Si. By annealing in furnace they will transform to metal silicide. Considering the metal-Si eutectic temperature, an a-Si thin film can be crystallized below 500°C. Consequently, the metal-induced crystallized (MIC) process is lower than SPC annealing temperature to get low temperature process. However, in spite of low crystallization temperature, metal contamination is a serious problem in MIC poly-Si. To improve its property, metal-induced lateral crystallization (MILC) process has demonstrated that high performance LTPS TFTs can be fabricated using Ni-MILC.

2.4 The Geometrical Correction Factor

A Hall device does not have to have a rectangular shape such as the example shown in Fig. 2-3, or indeed any other regular shape. Actually, any finite plate, provided with a least three contacts, may be used as a Hall device. Using conformal mapping theory, Wick demonstrated the invariance of Hall plate electrical efficiency with respect to geometry. However, some of the shapes may have some technological or application advantages over the others. For example, a vertical Hall device is much easier to fabricate in IC technology if all contacts are situated on one side of the plate. Alternatively, achieving a high value for the geometrical factor G in small-size devices is much easier in a cross-shaped configuration than in a rectangular one. Hall voltage of a Hall plate with an arbitrary shape can be expressed as

$$V_H = G V_{H\infty} \quad (2.19)$$

Where G is a parameter called the geometrical correction factor and $V_{H\infty}$ denotes the Hall voltage in a corresponding infinitely long strip. "Corresponding" means that the two devices have identical Hall coefficients and thicknesses, are biased by identical currents, and are exposed to identical homogeneous magnetic inductions. The geometrical correction factor summarily represents the diminution of the Hall voltage due to a non-perfect current confinement in a finite length Hall device. The geometrical correction factor is a number limited by $0 < G < 1$. For a very long Hall device, $G \sim 0$. The geometrical correction factor G is an important parameter of real Hall devices. To determine the value of G for a particular Hall plate shape, one must somehow calculate the Hall voltage for a plate of this shape V_H , and the Hall voltage of the corresponding infinitely long device $V_{H\infty}$. The geometrical correction factor is given by

$$G = V_H / V_{H\infty} \quad (2.20)$$

The Hall voltages for Hall plates of various shapes have been calculated using the following methods : conformal mapping techniques, boundary element methods, and finite difference or finite element approximations.

The influence of the shape of a Hall plate on the Hall voltage can be represented by the geometrical correction factor G . Briefly, this factor describes the diminution of the Hall voltage in a Hall device due to a non-perfect current confinement. The geometrical correction factor is defined by (2.20). The geometrical correction factor is a function of device geometry and the Hall angle. For a rectangular Hall plate with point sense contacts, such as that show in Fig.2-3 (a), the geometrical correction factor can be approximated as

$$G \cong 1 - \frac{16}{\pi^2} \exp\left(-\frac{\pi l}{2w}\right) \left[1 - \frac{8}{9} \exp\left(-\pi \frac{l}{w}\right)\right] \left(1 - \frac{\Theta_H^2}{3}\right) \quad (2.21)$$

This holds if $0.85 \leq l/w < \infty$ and $0 \leq \Theta_H \leq 0.45$

For a relatively long Hall plate, with $l/w > 1.5$ and small sense contacts $s/w < 0.18$, it was found for small Hall angles that

$$G \cong \left[1 - \frac{16}{\pi^2} \exp\left(-\frac{\pi l}{2w}\right) \frac{\Theta_H}{\tan \Theta_H}\right] \left(1 - \frac{2s}{\pi w} \frac{\Theta_H}{\tan \Theta_H}\right) \quad (2.22)$$

2.5 Basic characteristics

The normal component of the magnetic induction is then the input signal, and the Hall voltage is the output signal. We shall define and discuss the basic coefficients of a Hall device characterizing its operation as a magnetic induction/voltage transducer [9].

(a) Sensitivity S :

Sensitivity is the most important parameter of a sensor. In a modulating transducer such as a Hall device, we may define absolute sensitivity and relative sensitivity.

(1) absolute sensitivity :

$$S_A = \frac{V_H}{B} = \frac{GI_D r_{nch}}{Q_{ch}} \quad (2.23)$$

(2) supply voltage related sensitivity :

$$V = \frac{I}{qn\mu_n^*} \frac{L}{Wt} \quad V_H = \mu_n^* \frac{GW}{L} BV \quad S_V = \frac{V_H}{BV} = \mu_n^* \frac{GW}{L} \quad (2.24)$$

(3) current related sensitivity :

$$S_I = \frac{V_H}{BI} = \frac{R_H G}{t} = \frac{Gr_n}{qnt} \quad (2.25)$$

(b) Offset voltage V_{off} :

When a Hall effect transducer is biased, there will be a small voltage on the output even in the absence of a magnetic field. The offset voltage will limit the ability of the transducer to discriminate small steady-state magnetic fields. Some effects conspire to create this offset voltage, including misalignment of the sense contacts, inhomogeneous in the material of the transducer, and nonuniform thickness of the film. Besides, the materials used to make Hall effect transducers is highly piezoresistive, meaning that the electrical resistance of the material changes in response to mechanical distortion. This may cause most Hall effect transducers to behave like strain gauges in response to mechanical stresses imposed on them by the packaging and mounting.

(c) Noise voltage V_N :

The fundamental and unavoidable of electrical noises is called Johnson noise, and it comes from the thermally induced motion of charge carriers in a conductive material. It is a function of the operating temperature and the resistance of the device. Johnson noise is described by :

$$V_n = \sqrt{4kTRB} \quad (2.26)$$

where k is Boltzmann constant, T is absolute temperature, R is resistance, B is bandwidth

Besides, another noise called Flicker noise (or 1/f noise) is found in many physics systems, and can be generated by many different and unrelated types of mechanisms. The flicker noise developed by a transducer is related to the specific materials and fabrication techniques used. Then, we must consider the two kinds of noise simultaneously and call them V_N .

(d) SNR :

At a steady magnetic field, the signal-to-noise ratio is given by

$$SNR = \frac{V_{Hall}}{V_{off} + V_N} = \mu_n^* B \omega / \Delta l \quad (2.27)$$

where μ_n^* is Hall mobility, Δl is the geometrical offset of the sense contacts relative to an equipotential plane. Generally, it is proportional to carrier mobility.

2.6 Structure design

We can know that hall voltage is proportion to the geometry factor for semiconductor magnetic sensor from equation 2.28 and 2.29 is the induced charge from channel [10], [11].

$$V_H = G I_D B \frac{r_{nch}}{Q_{ch}} \quad (2.28)$$

$$Q_{ch} = C_{ox} (V_G - V_T) \quad (2.29)$$

We add two sensing electrodes on the structure of traditional thin film transistor. When the device is operated at biased voltage and simultaneously affected by a

magnetic field simultaneously, the potential will be measured by electrodes. Figure 2-2 shows the profile structure of Hall sensor. The potential will proportion to the applied magnetic field bias. On the other hand, the potential will arise when we applied higher bias current at constant magnitude of magnetic field. The magnitude of potential will saturate when the bias current up to a degree. At this time the carrier of inversion layer will not change their direction with different applied magnetic field. The size and location of electrodes will affect the magnitude of potential and sensitivity. Besides, the channel length and width will also have influence on the potential and sensitivity. In our study, we focus our study on the comparison of different channel length and width, the location of the sensing electrodes, and the geometry of structure. Figure 2-3 shows the different electrode designs of structure.



Reference

- [1] George Caruntu , Ovidiu Dragomirescu, “ Consideration regarding the offset of the magnetic sensors” , IEEE, 2002
- [2] G. K. Giust and T. W. Sigmon, “Low-Temperature Polysilicon Thin-Film Transistors Fabricated from Laser-Processed Sputtered-Silicon Films,” *IEEE Electron Device Lett.*, vol. 19, pp. 343-344, Sept. 1998.
- [3] N. Kubo, N. Kusumoto, T. Inushima, and S. Yamazaki, “Characterization of polycrystalline-Si thin-film transistors fabricated by excimer laser annealing method,” *IEEE Trans. Electron Devices*, vol. 40, pp. 1876-1879, Oct. 1994.
- [4] G. K. Giust and T. W. Sigmon, “High-Performance Laser-Processed Polysilicon Thin-Film Transistor,” *IEEE Electron Device Lett.*, vol. 20, no. 2, pp. 77-79, Feb. 1999.
- [5] G. Radnoczi, A. Robertsson, H. T. G. Hentzell, S. F. Gong, and M. A. Hasan, “Al induced crystallization in of a-Si,” *J. Appl. Phys.*, vol. 69, pp. 6394-6399, 1991.
- [6] S. W. Russel, Jian Li, and J. W. Mayer, “In situ observation of fractal growth during a-Si crystallization in a Cu_3Si matrix,” *J. Appl. Phys.*, vol. 70, pp. 5153-5155, 1991.
- [7] Bo Bian, Jian Yie, Boquan Li, and Ziqin Wu, “Fractal formation in a-Si:H/Ag/a-Si:H films after annealing,” *J. Appl. Phys.*, vol. 73, pp. 7402-7406, 1993.
- [8] Yunosuke Kawazu, Hiroshi Kudo, Seinosuke Onari, and Toshihiro Arai, “Low-temperature crystallization of hydrogenated amorphous silicon induced by nickel silicide formation,” *Jpn. J. Appl. Phys. Part1*, vol. 29, pp. 2698-2704, 1990.
- [9] S. M. Sze, *Semiconductor Sensors*, Wiley-Interscience, New York, 1994, p.240
- [10] S. Middelhoek, Audet S.A., “Physics of silicon sensors”, Academic Press, London, 1989.
- [11] R. Stere, I. Ristea, M. Bodea, *Tranzistoare cu efect de camp*, Editura Tehnica, Bucuresti, 1972.

Chapter 3

Experimental Procedure

3.1 The Fabrication Process Flow

The devices were fabricated on 4-inch-diameter p-type silicon wafer. Fig. 3-1 shows the process flow of the device. The 100nm undoped amorphous silicon (a-Si) films were initially deposited on 500nm thermally oxidized silicon (100) wafers by low-pressure chemical vapor deposition (LPCVD) system with silane (SiH_4) gas at 550°C . The deposition pressure was 100 mtorr and the silane flow rate was 40 sccm. Amorphous Si thin films anneal in furnace at 600°C several hours (~24 hr) to convert into polycrystalline form. After defining the device active areas, a 60 nm-thick TEOS oxide film was deposited at 350°C to serve as the gate dielectric by PECVD. Then, a 300 nm thick poly-Si was deposited by LPCVD at 600°C with SiH_4 for the gate electrode. Gate areas were patterned and the regions of source, drain, and gate electrode were doped by a self-aligned 5×10^{15} ions/ cm^2 phosphorus implantation with a He-diluted PH_3 gas, at 50 KeV of acceleration voltage. The dopant were activated at 600°C in N_2 ambient for 24 hr. Next, a 500nm TEOS oxide was deposited by PECVD at 350°C as a passivation layer, and contact lithography was carried out. After opening contact holes, a 500 nm Al was deposited by evaporation and the metal layer was patterned. Finally, the samples were sintered at 400°C for 30min in N_2 gas ambient.

The conventional Hall sensors which use inversion layer as sensing layer has three disadvantages compared with bulk Hall sensor, including lower channel mobility, surface instability, and larger $1/f$ noise. In order to improve the performance of the device, we have to lower defects of the channel to add carrier mobility, avoid misalignment of the sense contacts to decrease offset voltage, and decrease contact resistance. The detailed fabrication process flow is listed as follows :

1. (100) orientation Si wafer
2. Initial cleaning
3. Thermal wet oxidation at 1050°C to grow 5000\AA thermal oxide in furnace
4. 1000\AA a-Si was deposited by LPCVD at 550°C in SiH_4 gas
5. Amorphous Si thin films anneal in furnace at 600°C several hours (~24 hr)

to convert into polycrystalline form

6. Mask#1: define active regions (poly-Si dry etch by Poly-RIE system)
7. RCA cleaning
8. 600 Å gate dielectric deposition by PECVD at 350 °C
9. 3000 Å poly-Si was deposited by LPCVD at 620 °C in SiH₄ gas
10. Mask#2: Define gate regions (poly-Si dry etch by Poly-RIE system)
11. Ion implantation: P³¹, 50KeV, 5x10¹⁵ ions/ cm²²
12. Dopant activation in N₂ ambient at 600 °C for 24hrs in furnace
13. 5000 Å TEOS oxide was deposited by PECVD as passivation layer
14. Mask#3: Open contact holes
15. 5000 Å Al thermal evaporation
16. Mask#4: Al pattern defined
17. Etching Al and removing photoresist
18. Al sintering at 400 °C in N₂ ambient for 30 min

Only four masking steps and one implant step are required to fabricate our proposed Hall effect magnetic sensors. The proposed devices are entirely controlled low temperature, lower than 600°C. A polycrystalline layer can be considered as monocrystalline grains separated by grain boundaries. Trapped charges in these grain boundaries create an energy barrier. These barriers limit the carrier mobility in the film. In order to decrease grain boundary, the active layers are amorphous and crystallized by a thermal annealing to obtain a polycrystalline film. Besides, we adopt the self-aligned method to avoid misalignment of the device. So we only need the same mask to define source, drain, gate, and Hall probes. Thus, we can accurately control the positions of source, drain, and probes to discuss the relation between the geometrical factor and the performance of the Hall sensor.

In this thesis, our study process flow is listed as follows :

1. assemble information for a experiment
2. design the structure of the proposed devices
3. layout the fabricated process of the device
4. draw the mask
5. the fabrication of the mask
6. the fabrication of the sensor

7. measurement of the sensor based on TFT
8. measurement of the magnetic sensor with Hall effect
9. analysis data and information
10. optimize different kinds of the sensing devices

3.2 Measurements

3.2.1 Electronic Bench Equipment

We measured the I-V characteristics by HP4156 semiconductor parameter analyzer with five probe stages at room temperature. And we apply magnet to constant magnetic field. All the Hall effect measurements are made at a magnetic field of 0.2 Tesla and V_H is extracted from a mean of three measurements. Fig. 3-3, 3-4 show the schematic of the measurements. We use five probes to contact source, drain, gate, and two pads. The source side is ground while drain and gate side are applied some voltage. Two pads are read pad-source voltage and determine the Hall voltage.

We must consider the offset voltage and we may get the actual Hall voltage [1], [2]. In ideal case, there is no difference between two sensing pad. However, there are some experiment errors, including misalignment of the sense contacts, inhomogeneous in the material of the transducer, nonuniform thickness of the film, nonuniform quantity of the dopant. And they will produce offset voltage between two sensing pads [3].

3.2.2 Magnetic Instrumentation

A gaussmeter measures magnetic flux density (B) at a given point in space. Most gaussmeters employ Hall effect sensor elements as the magnetic probe [4]. In its simplest form, a gaussmeter is a linear Hall effect sensor with a meter readout. A few of the features to look for in a gaussmeter are :

- (1) range – How small, and how large a field can it measure?
- (2) accuracy – To what degree does the reading reflect reality?
- (3) interface options – In addition to a front-panel display, can it communicate with PCs or other instruments?

Range is important because there are times when you will want to measure fields of a few gauss, and others where you will want to measure fields of several

kilogausses. The need for accuracy needs little, if any, elaboration. Inaccurate instruments can make your life vastly more difficult. Accurate instruments, regularly calibrated, can make development work go more smoothly by reducing one potential source of errors.

We place our devices between two magnets and magnetic field is perpendicular to our devices. We control the distance of the magnets to maintain magnetic field of 0.2 Tesla and use gaussmeter to measure the magnetic flux density (B).



Reference

- [1] Yishay Netzer, A Very Linear Noncontact Displacement Measurement with a Hall Element Magnetic Sensor, Proceeding of the IEEE, vol, 69, No. 4, p.491, 1981
- [2] Major, R.V. "Current measurement with magnetic sensors" Magnetic Materials for Sensors and Actuators (Digest No. 1994/183), IEE Colloquium on 11 Oct. 1994 Page(s):5/1 - 5/3
- [3] R. S. Popovic, "Hall effect devices," Sens. Actuators 17, 39 (1989).
- [4] Sensors : a comprehensive survey : magnetic sensors/Gopel, W. & Hesse, J. & Zemel, J. N. ed. New York/VCH/c1989



Chapter 4

Results and Discussion

In this chapter, we will discuss the device performance of our proposed magnetic sensor. We measured the I-V characteristics by HP4156 semiconductor parameter analyzer. All the Hall effect measurements are made at a magnetic field of 0.5 Tesla and V_H is extracted from a mean of three measurements.

4.1 Transistors Characteristics

4.1.1 The output characteristics of our proposed magnetic sensor

Fig. 4-1, 4-8, 4-12 show I_{ds} - V_{ds} output characteristics of our proposed magnetic sensor based on TFT structure with varies V_{gs} following the well square law of a standard thin film transistor under general measuring environment (without magnetic field applied), And we can find that I_{ds} is not obvious until the V_{gs} arise to 20 V. Obviously, there is no kink effect when V_{ds} arise to 30 V. It is because that the kink current in TFT devices is basically due to the avalanche or impact ionization in the device and is strongly influenced by grain boundary traps. The grain boundary traps can prevent the channel carriers from gaining higher energy, and therefore the impact ionization probability can be reduced as the grain trap density is increased [1]. It is well know that the grain boundary trap density of SPC is usually higher than that of ELA or other recrystallization methods. Therefore, the TFT device with SPC method has higher carrier mobility and less kink effect.

4.1.2 The transfer characteristics of our proposed magnetic sensor

Fig. 4-2, 4-9, 4-13 show the transfer characteristics of our proposed magnetic sensors based on TFT structure under general measuring environment (without magnetic field applied). Here we can find that the off leakage current I_{ds} increase with the arising bias voltage V_{ds} . There is less difference on the saturation currents regime on device 1 but much difference on device 3 and device 4. The main reason for lower off-state leakage current of the TFT device with low drain voltage is that the drain electric field is lower and hot carrier effect is less serious [2]. The best on/off current

ratio on device 1 is more than 7 orders in logarithm scale and 6 orders in logarithm on device 3 and device 4. The on-off current ratio is defined as that ratio of the maximum turn-on current to the minimum off-state current. Besides, the four kinds of device have different turn-on current due to different W/L value.

4.2 Sensors Characteristics

4.2.1 The comparison of the Hall voltage versus V_{ds}

Fig. 4-3 shows the comparison of the Hall voltage versus V_{ds} for varies V_{gs} at 10V to 30 V in steps with $W/L = 80 \mu\text{m}/150 \mu\text{m}$ and sensing pad is closed to source with the $35 \mu\text{m}$. In this figure, we find there is a peak value of each characteristic curves. The first peak value happened in the curve of V_{gs} at 10V, corresponding to the V_{ds} at 1.3V. The peak positions corresponding to the V_{ds} shift to be larger as the V_{gs} increasing. The maximum peak value happened at the V_{gs} with 15V, and then decrease with the V_{gs} increasing. The peak values appear at some gate and drain voltage. In the linear region, the Hall voltage arises with the V_{ds} increasing and this is because the Hall voltage is dependent of drain current. The Hall voltage decreases with the V_{ds} increasing in the saturation region of the drain current. We think the carrier accumulating pad may be attracted due to electric field between sensing pad and drain. The amount of the attracted carriers is more than that of the accumulated carriers. So the Hall voltage decreases deeply. Due to the sensing pad is closed to source, the voltage gap between sensing pad and drain is larger to absorb carriers accumulating pad easily.

Fig. 4-6 shows comparison of the Hall voltage versus V_{ds} for $V_{gs} = 15\text{V}$, 20V, 25V, 30V, $W/L = 80 \mu\text{m}/150 \mu\text{m}$, and the sensing pad is closed to drain with the $35 \mu\text{m}$. In this figure, the characteristics are quasi linear for smaller drain voltages and saturate for higher drain voltage. There are smaller peaks in this condition. In other words, when the sensing pad is closed to drain, there are smaller peaks. The peak positions corresponding to the V_{ds} shift to be larger as the V_{gs} increasing. The smaller peaks may arise from smaller voltage gap between sensing pad and drain due to the sensing pad is closed to drain. In the linear region, V_H decrease with gate voltage increasing and drain voltage arriving saturation is higher for higher gate

voltage. The carrier concentration will increase as gate voltage increases. Thus, V_H will decrease in this condition. In other words, the carrier concentration is dominant factor influenced V_H in this device.

Fig. 4-10 shows comparison of the Hall voltage versus V_{ds} for $V_{gs} = 10V, 15V, 20V, 25V, 30V$ with $W/L = 40 \mu m/100 \mu m$ and the sensing pad is closed to source with the $20 \mu m$. Like Fig. 4-3, it also has peak Hall voltage values when the sensing pad is closed to source. But the peaks are smaller than those in Fig. 4-3. This device is shorter so the voltage gap between sensing pad and grain is smaller. Thus, the attractive ability is smaller than device 1. Besides, we can find the Hall voltage versus V_{ds} presents oscillation. The voltage gap between sensing pad and drain is smaller so the accumulating carrier can compensate the lost attracting carriers. The carrier mobility is proportion to gate voltage and then the current will increase as gate voltage increases. So we can find the Hall voltage is higher as gate voltage increases. We think the Hall voltage arriving saturation is higher for higher drain voltage and drain current arriving saturation is also higher for higher gate voltage. Drain current arriving saturation shows no more carriers run to sensing pad and directly transport to drain.

Fig. 4-14 shows comparison of the Hall voltage versus V_{ds} for $V_{gs} = 10, 15, 20, 25, 30 V$ and $W/L = 40 \mu m/100 \mu m$ and the sensing pad is closed to drain with the $20 \mu m$. From this figure, there is no peak in lower gate voltage. We think this is related to the channel length of this device. This device is shorter so the voltage gap between sensing pad and drain is smaller to keep the carriers at the sensing pad.

So we can find that there are two kinds of type in Hall voltage variation accompany with the increasing of drain voltage. The first one appears large peak type of Hall voltage when sensing pad is closed to source. The second type of Hall voltage appears rising with the increasing of drain voltage V_{ds} initially, and the following is smaller oscillation after some critical V_{ds} when sensing pad is closed to drain.

4.2.2 The voltage of sensing electrode pad varies with time

Fig.4-4, 4-5 show the voltage of sensing electrode pad varies with time with/without magnetic field bias and Hall voltage versus time for some V_{gs} and V_{ds} .

We find V_H decreases with time increasing and then saturates subsequently. V_{sr} is voltage with/without magnetic field and V_H is Hall voltage. The relation between V_{sr} and V_H is [3]

$$V_H = V_{sr} (\text{with } B) - V_{sr} (\text{without } B)$$

Where B is magnetic field

Fig. 4-5 can demonstrate the Hall voltage decreases with the V_{ds} increasing in the saturation region of the drain current in Fig. 4-3. We apply 100 seconds to observe the change of the Hall voltage and we find the Hall voltage is not constant. The Hall voltage is higher initially and lower eventually due to the accumulating carriers are attracted by electric field between sensing pad and drain. In addition, we also find the time of arriving saturation is longer at higher gate voltage.

Fig.4-7 shows the voltage of sensing electrode pad varies with time with/without magnetic field bias and Hall voltage versus time for $V_{gs} = 25V$, $V_{ds} = 15V$. This figure also can explain why there are peaks in Fig. 4-6.

Fig. 4-11 shows the voltage of sensing electrode pad varies with time with/without magnetic field bias and Hall voltage versus time for different drain and gate voltage with $W/L = 40 \mu m/100 \mu m$ and the sensing pad is closed to source with the $20 \mu m$. We can easily find the Hall voltage increases with the gate and drain voltage increasing in the linear region.

4.2.3 The offset voltage V_{off}

We take Fig. 4-15, 4-16, 4-17, 4-18, and 4-19 examples to explain how we get the Hall voltage as the offset voltage exists.

Fig. 4-15 shows the voltage difference of sensing electrode pad varies with time with/without magnetic field bias and Hall voltage versus V_{ds} for $V_{gs} = 10, 15, 20, 25, 30 V$ and $W/L = 40 \mu m/100 \mu m$ and sensing pad is closed to drain with the $20 \mu m$. There are five groups having different gate voltage in this figure and every group has four curves. $V_{sensing}$ is the voltage difference of the sensing pad with and without magnetic field and $V_{sensing}$ is larger with gate voltage increasing.

Fig. 4-16 shows the partial region of the Fig. 4-16 as $V_{gs} = 20V$. The black curve is voltage of the first sensing pad without magnetic field and blue curve is that of the second pad without magnetic field. We can find there is voltage gap between the two Hall probes and the gap increases with drain voltage increasing. And we call

this offset voltage V_{off} [4], [5]. Fig. 4-18 shows comparison of the offset voltage versus V_{ds} for $V_{gs} = 10, 15, 20, 25, 30$ V. The red curve is voltage of the first contact pad with magnetic field and the green curve is that of the second pad. The red curve shifts upward and the green one does downward. The shift degree increases with drain voltage increasing. From this figure, we know the second pad is accumulated by electron carriers. Thus, the voltage of the second pad with magnetic field is lower than that without magnetic field. Fig. 4-14 shows the voltage difference between the black and red curves and Fig. 4-17 shows the voltage difference between the blue and green curves. Then, the Hall voltage is the mean of the two V_H values. If we neglect the offset voltage, we would get wrong Hall voltage as Fig. 4-19.



Reference

- [1] Kow Ming Chang, Yuan Hung Chung, Gin Ming Lin, Jian Hong Lin and Chi Gun Deng, “ A novel high-performance poly-silicon thin film transistor with a self-aligned thicker sub-gate oxide near the drain/source regions,” IEEE Electron Device Letters, vol. 22, no. 10, p. 472, 2001.
- [2] M. Koyanagi, H. Kurino, T. Hashimoto, H. Mori, K. Hata, Y. Hiruma, T. Fujimori, I-Wei Wu and A. G. Lewis, “Relation between hot-carrier light emission and kink effect in poly-Si thin film transistors” IEEE 1991
- [3] R. S. Popovic, "Hall effect devices," Sens. Actuators 17, 39 (1989)
- [4] Carvou, E.; Le Bihan, F, “Hall effect magnetic sensors based on polysilicon TFTs”, Sensors Journal, IEEE, Volume: 4, Issue: 5, pp.597 – 602, 2004.
- [5] Doyle, J, “High sensitivity silicon magnetic field detector”, Custom Integrated Circuits, IEEE Conference, pp.105 – 108, 2001.



Chapter 5

Conclusions and future work

5.1 Conclusion

The thin film transistor magnetic sensors were fabricated completely with several kinds of geometric structure patterns and different dimensions. Characteristics of sensor devices with different measuring environments are analyzed and discussed. We can get effective Hall voltage under the magnetic field bias. Magnetic field strength changes the carriers' behavior in the semiconductor and induces the semiconductor devices appear different electrical characteristics [1].

Different geometric structures appear different magnetic sensitivity under the same space field strength [2]. We also find that the Hall voltage of the sensor pads in the thin film transistor responds with individual operation conditions. Gate bias and Drain voltage are the main two parameters in these experiments. There are two kinds of type in Hall voltage variation accompany with the increasing of Drain voltage. The first one appears the peak type of Hall voltage. The second type of Hall voltage appears rising with the increasing of drain voltage V_{ds} initially, and the following is smaller oscillation after some critical V_{ds} .

Before the Gate bias is less than the threshold voltage, the Hall voltage appears the oscillation wave type with the increasing of Drain voltage. It is due to the carrier electrons accumulated and discharged in the sensing pad alternatively. The accumulated charge will increase the Hall voltage, but the increasing drain voltage will attract the accumulated charge as the drain current. Then, the Hall voltage will turn down immediately.

5.2 Future work

The Semiconductor magnetometers fabricated embedded with thin film transistor by our design mentioned above could provide well sensing analyzability. We will

design different shapes of the Hall sensing layer and study the relation between sensitivity and shape. Thus, we can choose the suitable structures to the application of Hall sensors to every life. Furthermore characteristics of TFT magnetic sensor are not well known, especially how do the magnetic field affect the electrical variety in TFT. Semiconductor sensors can be applied in many kinds of family and industry applications. Relative process technology should be developed completely. We are deep interesting in optical, electrical and magnetic interactions in semiconductor micro structures. We believe that these technologies would extend and change our life mode in the future. How to integrate the magnetic sensor with other application circuits including some micro electro-mechanical systems in a unit chip is the most difficult challenge.



Reference

- [1] "Hall effect in semiconductors" Safa Kasap, Department of Electrical Engineering University of Saskatchewan, Canada
- [2] R. S. Popovic, "Hall effect devices," Sens. Actuators 17, 39 (1989)



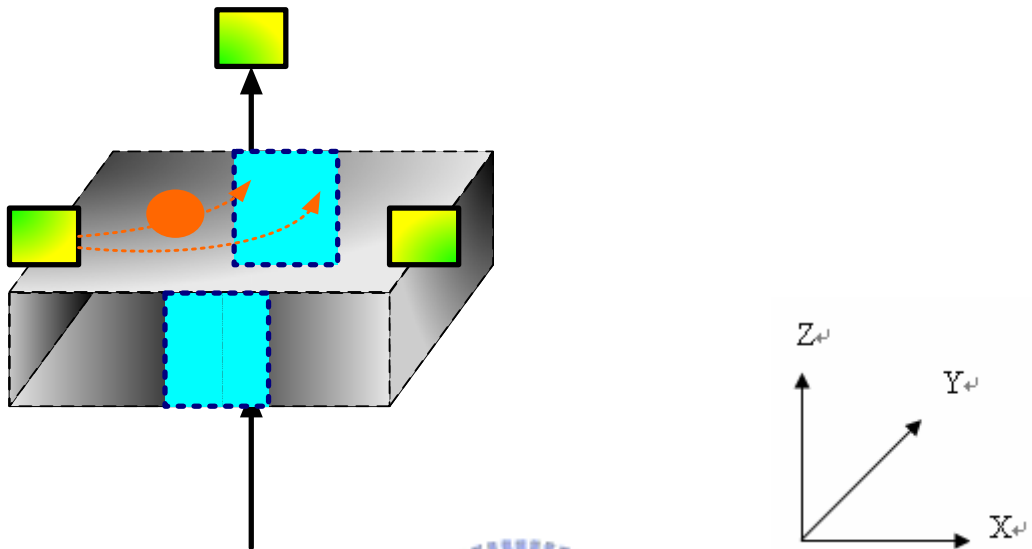


Fig. 2-1 The schema of the Hall effect in bulk

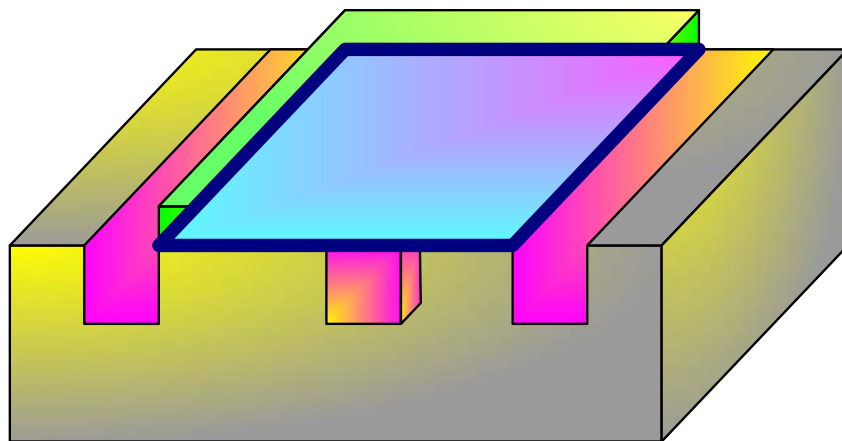


Fig. 2-2 the profile structure of Hall sensor

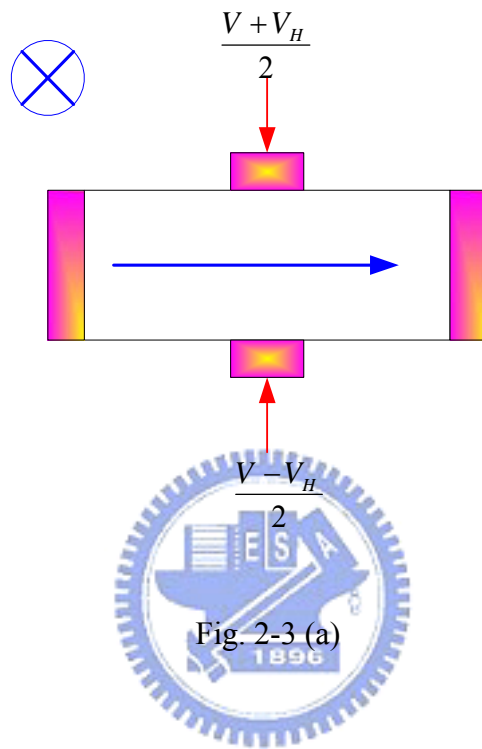


Fig. 2-3 (a)

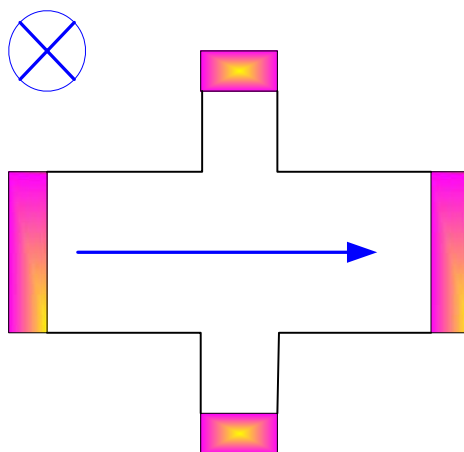


Fig. 2-3 (b)

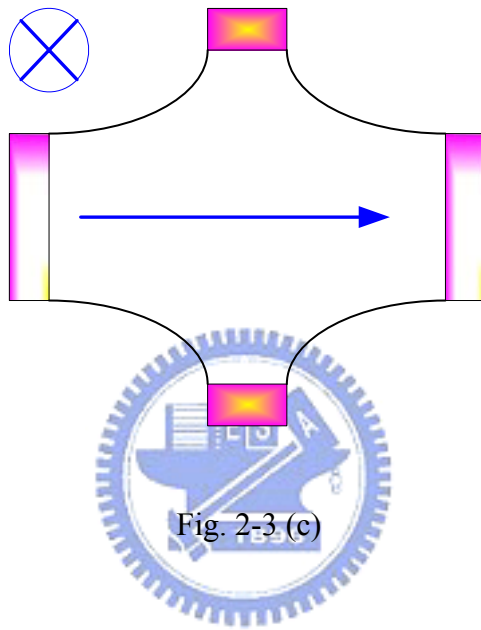


Fig. 2-3 (c)

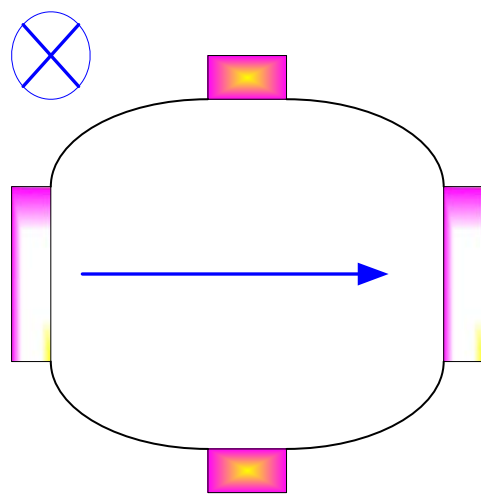


Fig. 2-3 (d)

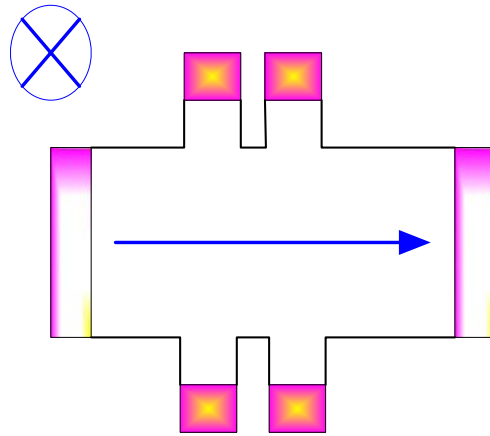


Fig. 2-3 (e)

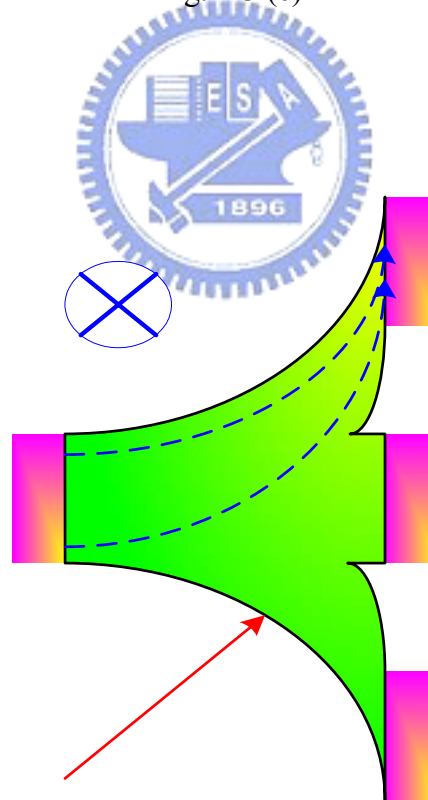
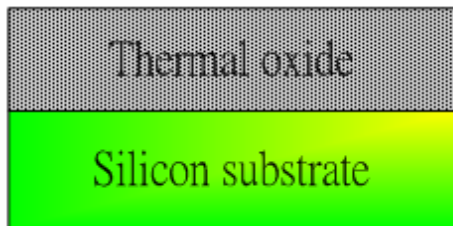
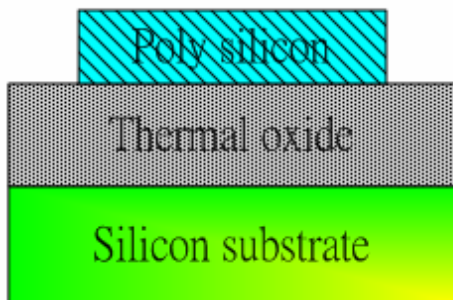


Fig. 2-3 (f)

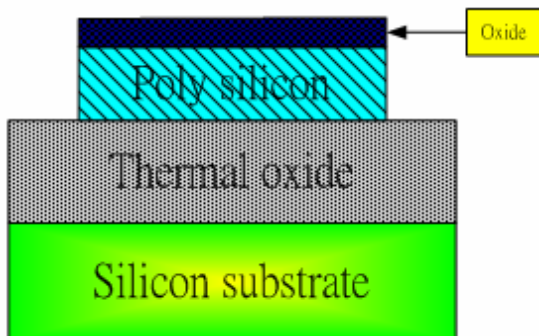
Fig. 2-3 the different electrode designs of structure



(a) Thermal oxidation



(b) LPCVD a-Si, recrystallization, and define active layer



(c) Deposit SiO₂ dielectric by PECVD

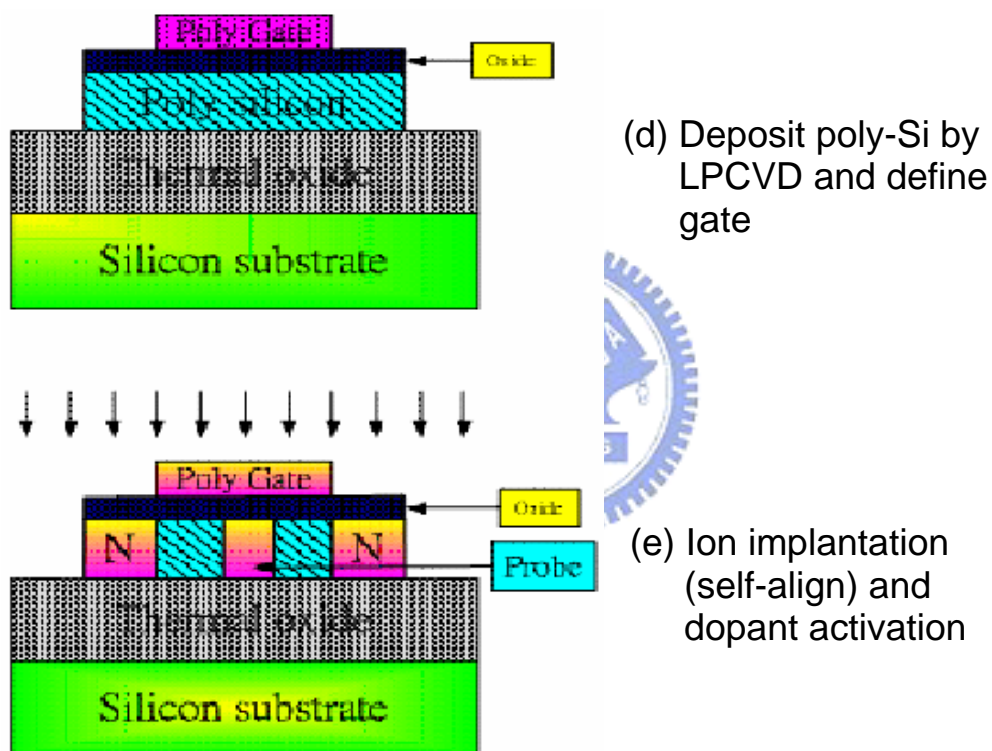


Fig. 3-1 Process flow of fabricating proposed magnetic field sensor

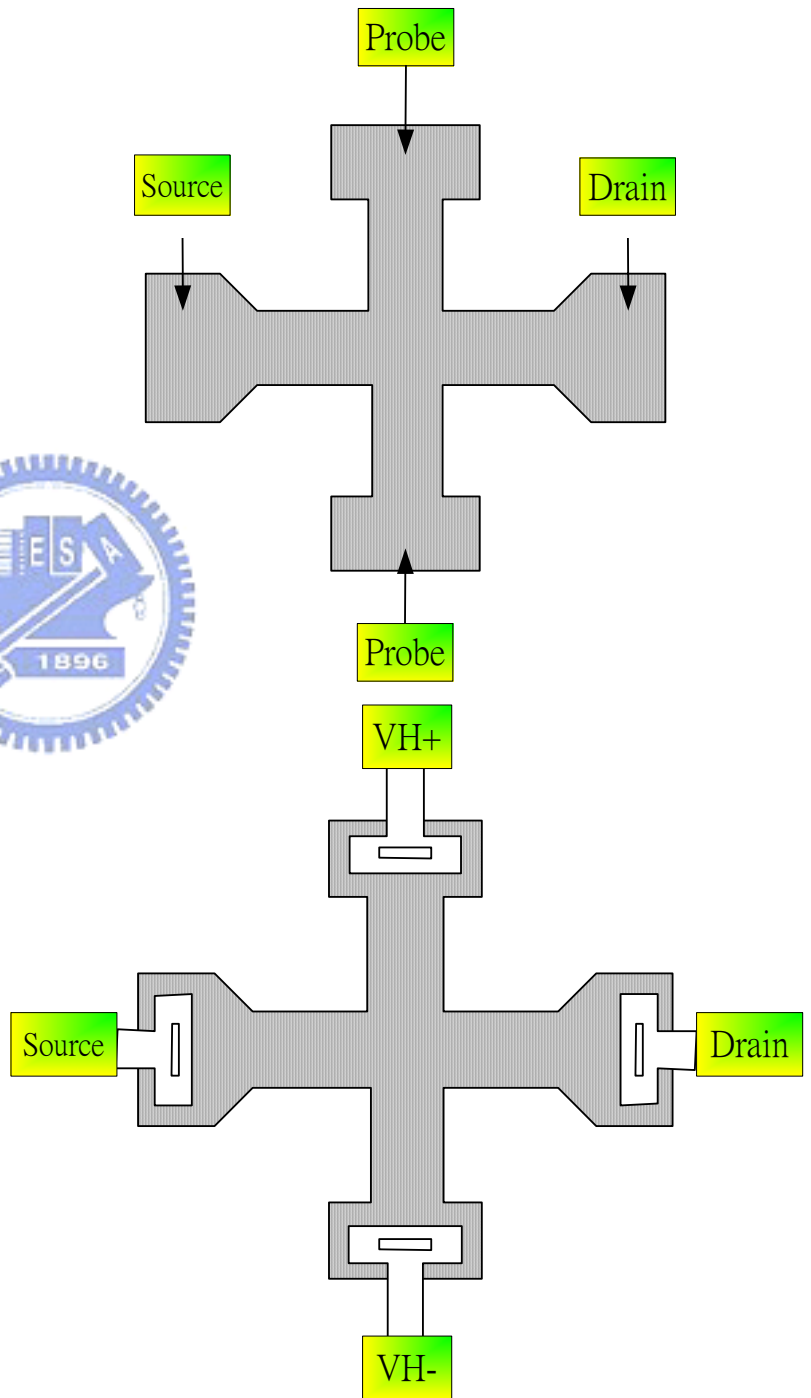
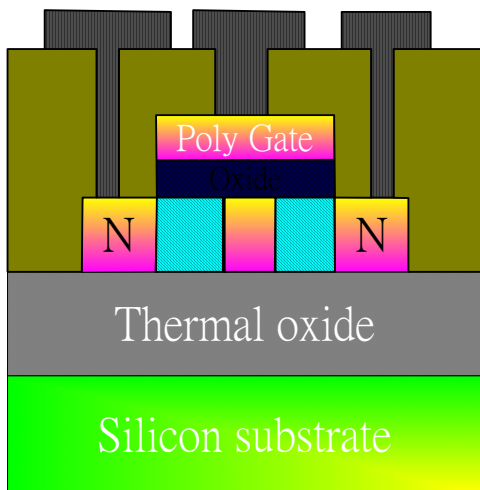
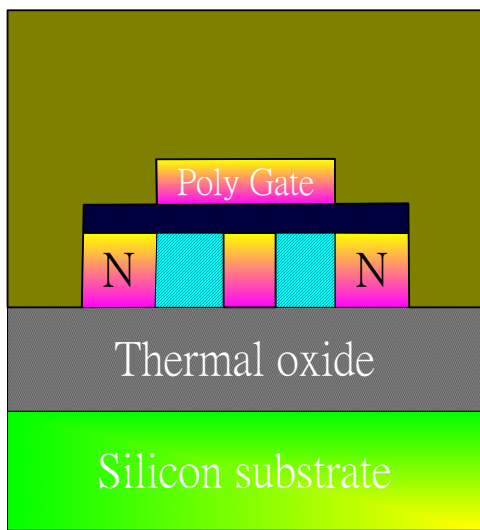
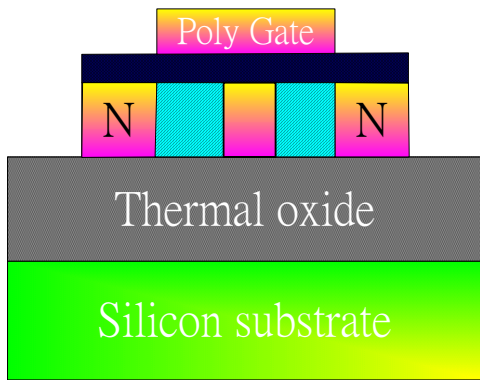


Fig. 3-2 Profile schematic of the Hall sensor

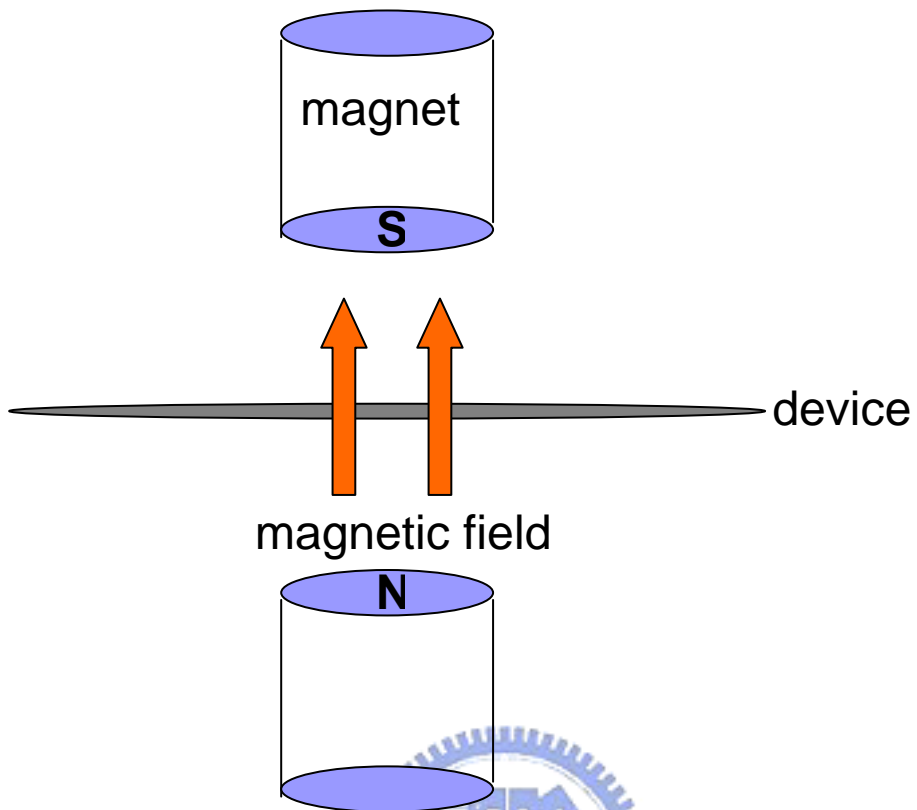


Fig. 3-3 The schematic of the measurement

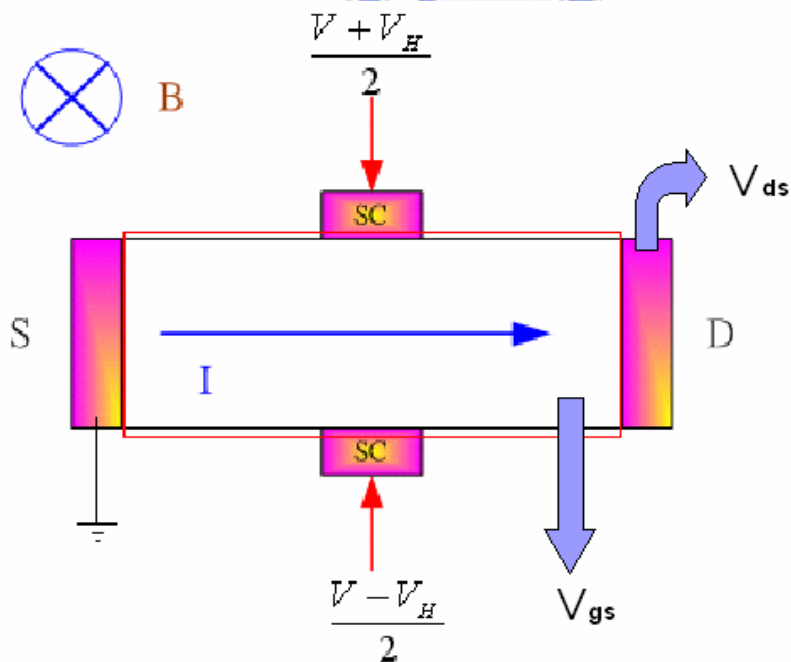


Fig. 3-4 The schematic of applied voltage

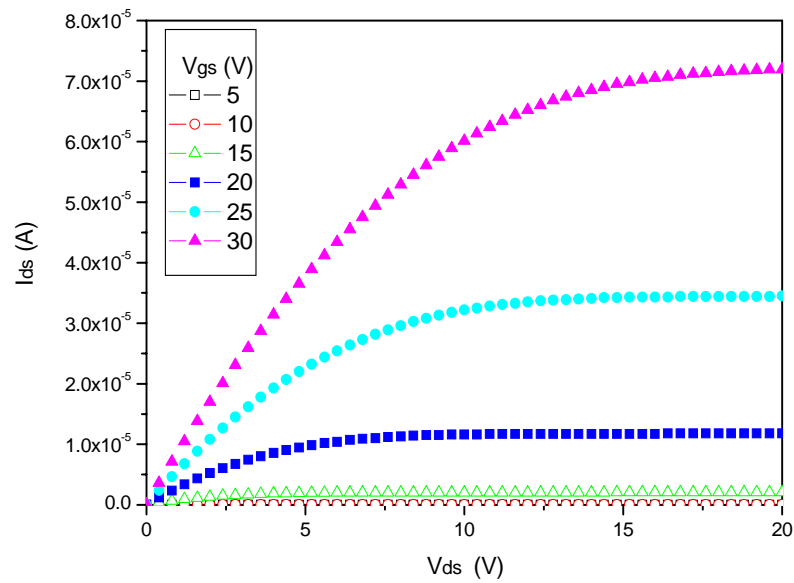


Fig. 4-1 I_{ds} - V_{ds} output characteristics of our proposed magnetic sensor based on TFT structure with versus V_{gs} ; $W/L = 80 \mu\text{m}/150 \mu\text{m}$; sensing pad is closed to source with the $35 \mu\text{m}$

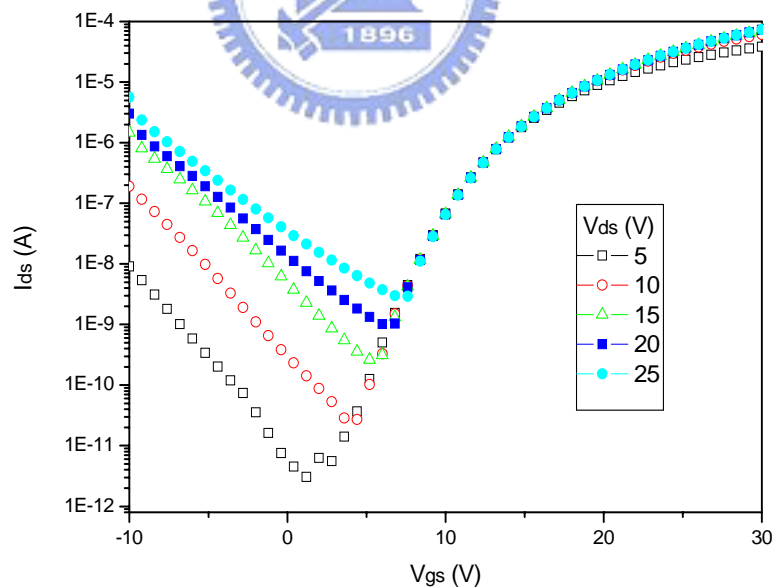


Fig. 4-2 I_{ds} - V_{gs} transfer characteristics of our proposed magnetic sensor based on TFT structure for $V_{ds} = 5, 10, 15, 20, 25$ V ; $W/L = 80 \mu\text{m}/150 \mu\text{m}$; sensing pad is closed to source with the $35 \mu\text{m}$

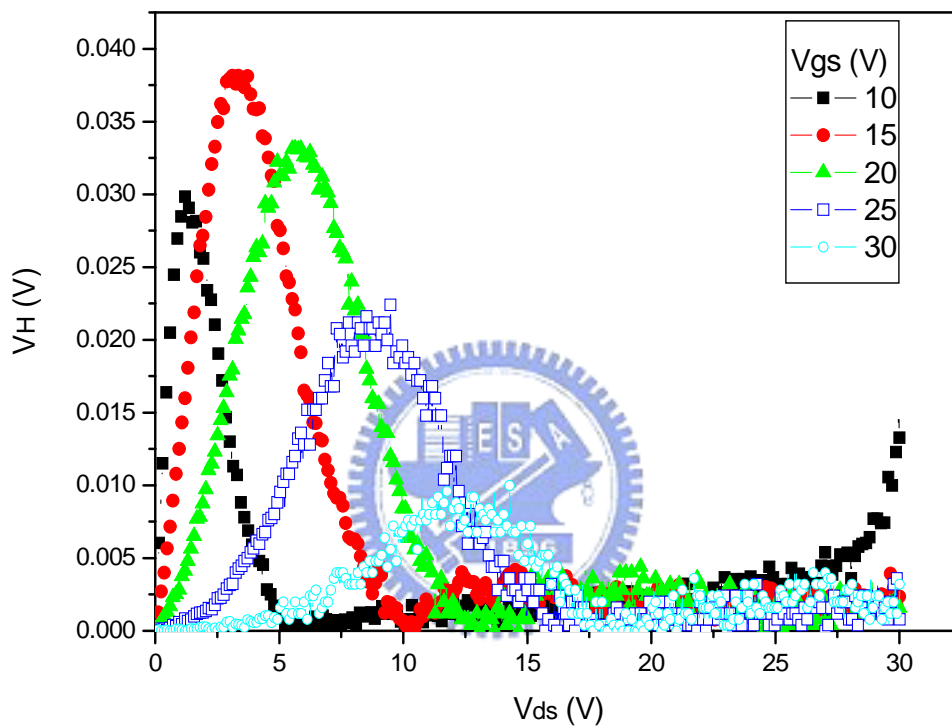


Fig. 4-3 Comparison of the Hall voltage versus Vds for Vgs = 10,15,20,25,30 V ; W/L = 80 μ m/150 μ m ; sensing pad is closed to source with the 35 μ m

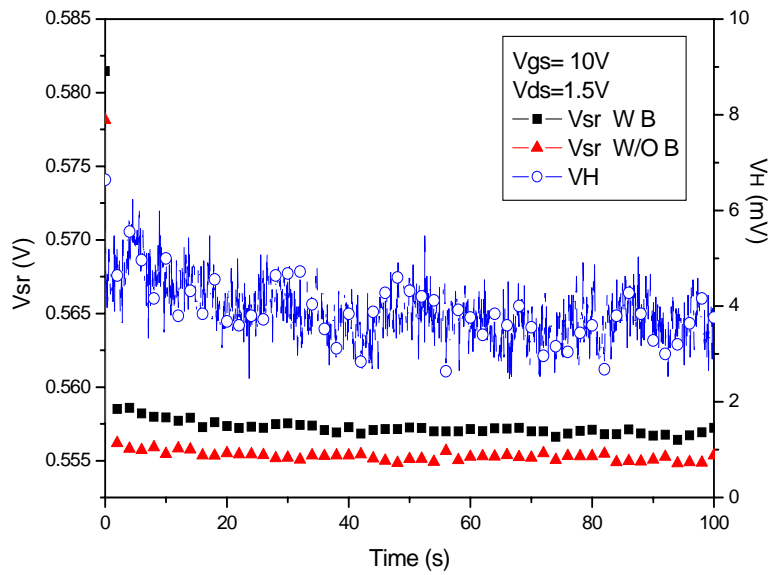


Fig. 4-4 The voltage of sensing electrode pad varies with time with/without magnetic field bias and Hall voltage versus time for $V_{gs} = 15V$, $V_{ds} = 3.5V$; $W/L = 80 \mu m/150 \mu m$; sensing pad is closed to source with the $35 \mu m$

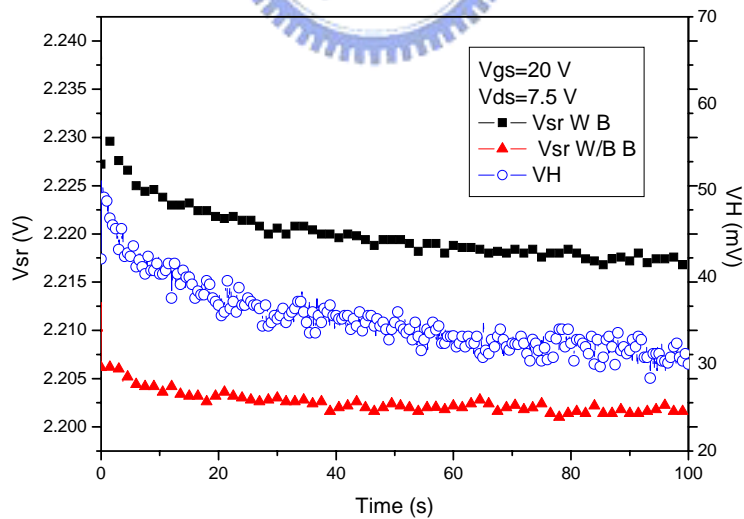


Fig. 4-5 The voltage of sensing electrode pad varies with time with/without magnetic field bias and Hall voltage versus time $V_{gs} = 20V$, $V_{ds} = 7.5V$; $W/L = 80 \mu m/150 \mu m$; sensing pad is closed to source with the $35 \mu m$

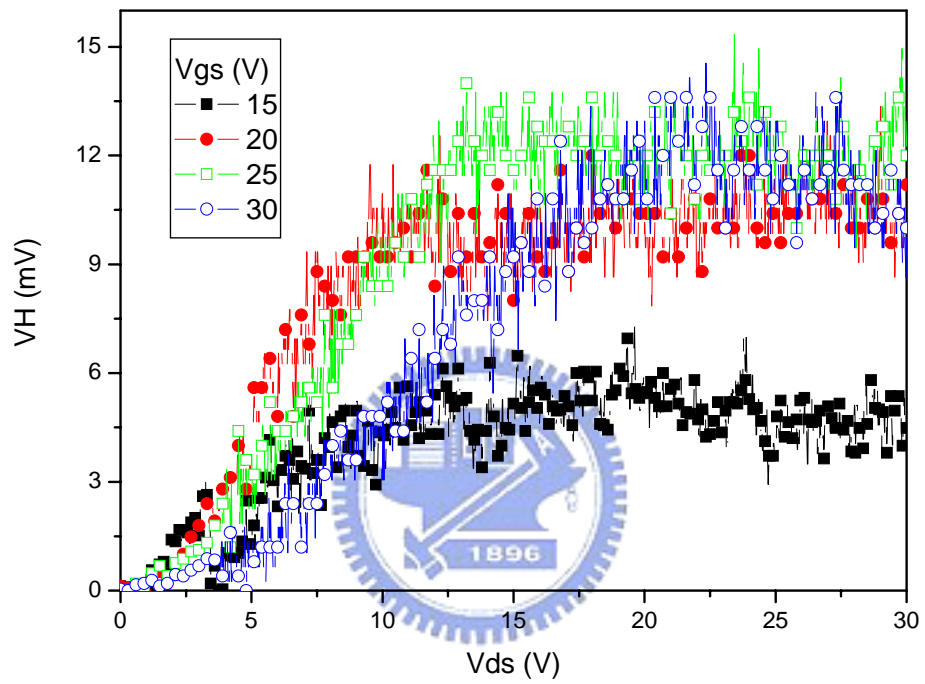


Fig. 4-6 Comparison of the Hall voltage versus Vds for Vgs = 15,20,25,30 V ; W/L = 80 μ m/150 μ m ; sensing pad is closed to drain with the 35 μ m

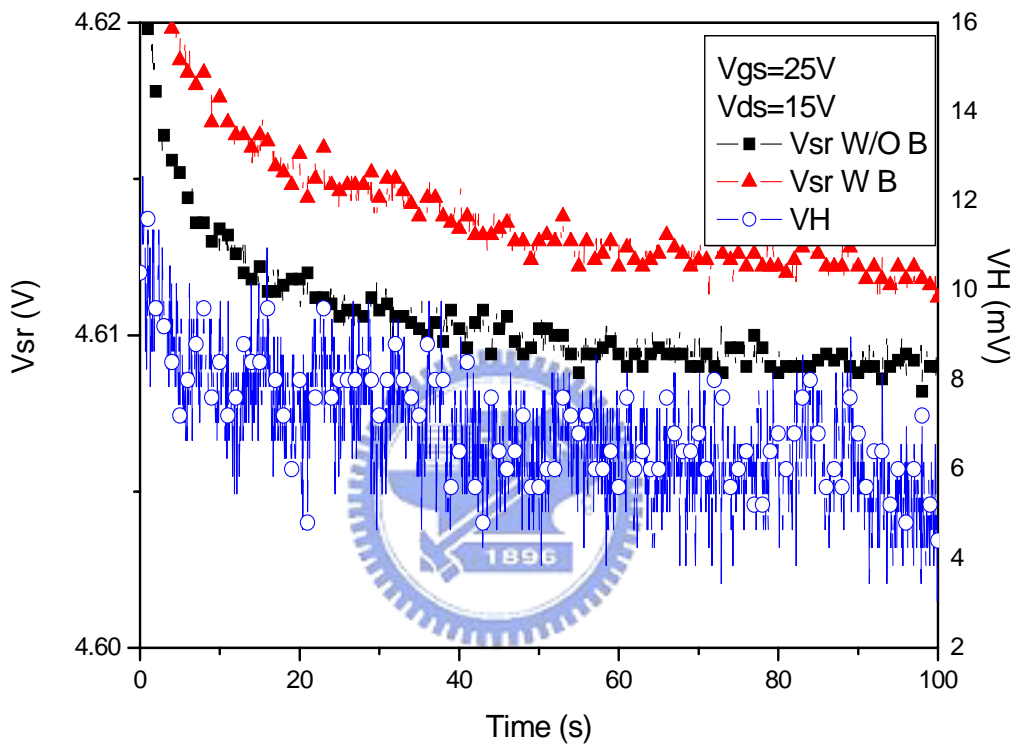


Fig. 4-7 The voltage of sensing electrode pad varies with time with/without magnetic field bias and Hall voltage versus time for $V_{gs} = 25V$, $V_{ds} = 15V$; $W/L = 80 \mu m/150 \mu m$; sensing pad is closed to drain with the $35 \mu m$

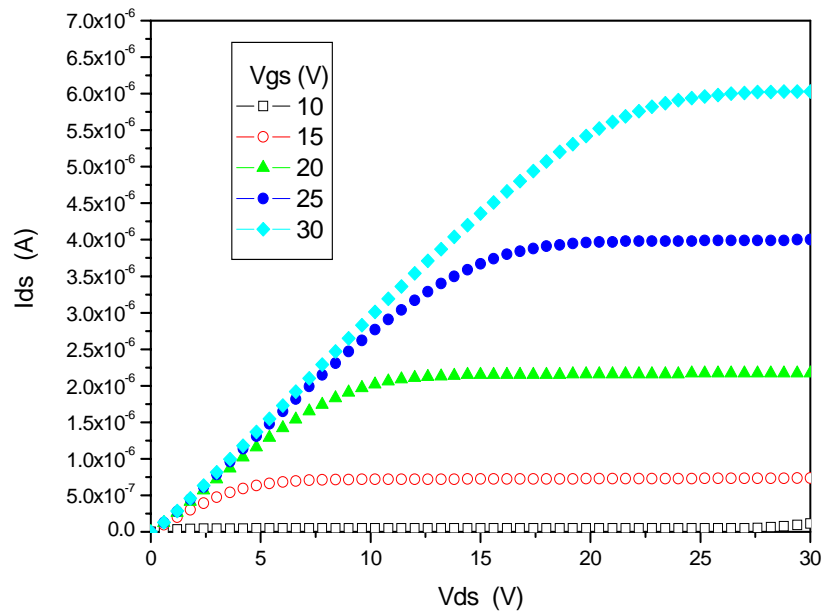


Fig. 4-8 I_{ds} - V_{ds} output characteristics of our proposed magnetic sensor based on TFT structure with versus V_{gs} ; $W/L = 40 \mu\text{m}/100 \mu\text{m}$; sensing pad is closed to source with the $20 \mu\text{m}$

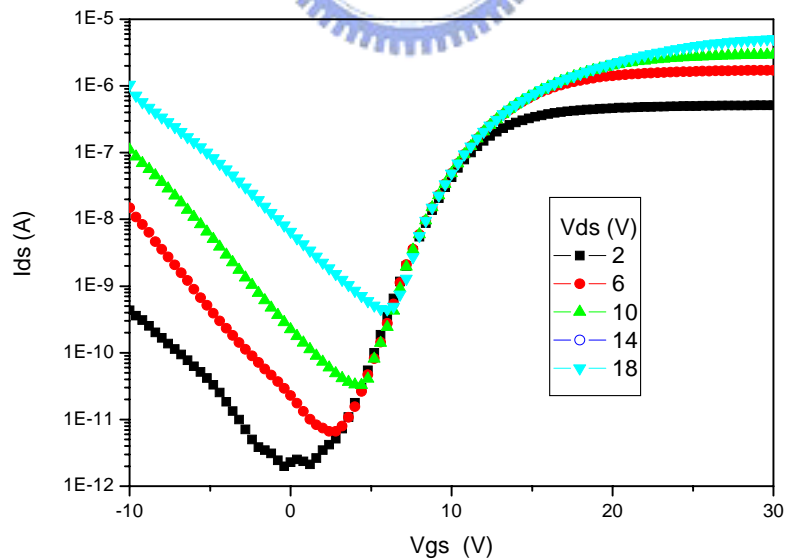


Fig. 4-9 I_{ds} - V_{gs} transfer characteristics of our proposed magnetic sensor based on TFT structure for $V_{ds} = 2, 6, 10, 14, 18$ V ; $W/L = 40 \mu\text{m}/100 \mu\text{m}$; sensing pad is closed to source with the $20 \mu\text{m}$

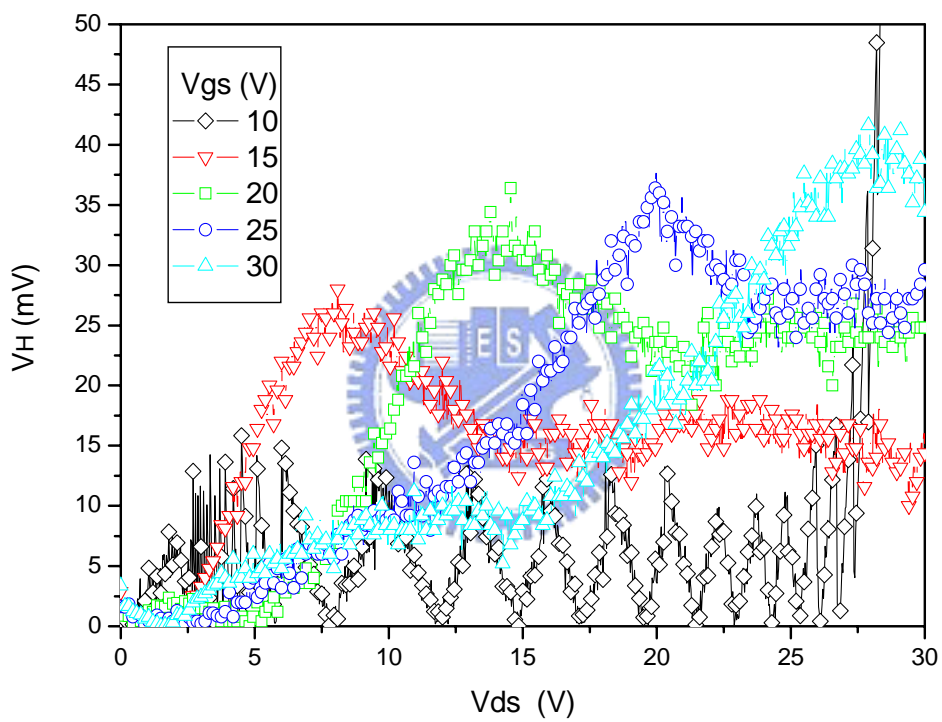


Fig. 4-10 Comparison of the Hall voltage versus V_{ds} for $V_{gs} = 10, 15, 20, 25, 30$ V ; $W/L = 40 \mu\text{m}/100 \mu\text{m}$; sensing pad is closed to source with the $20 \mu\text{m}$

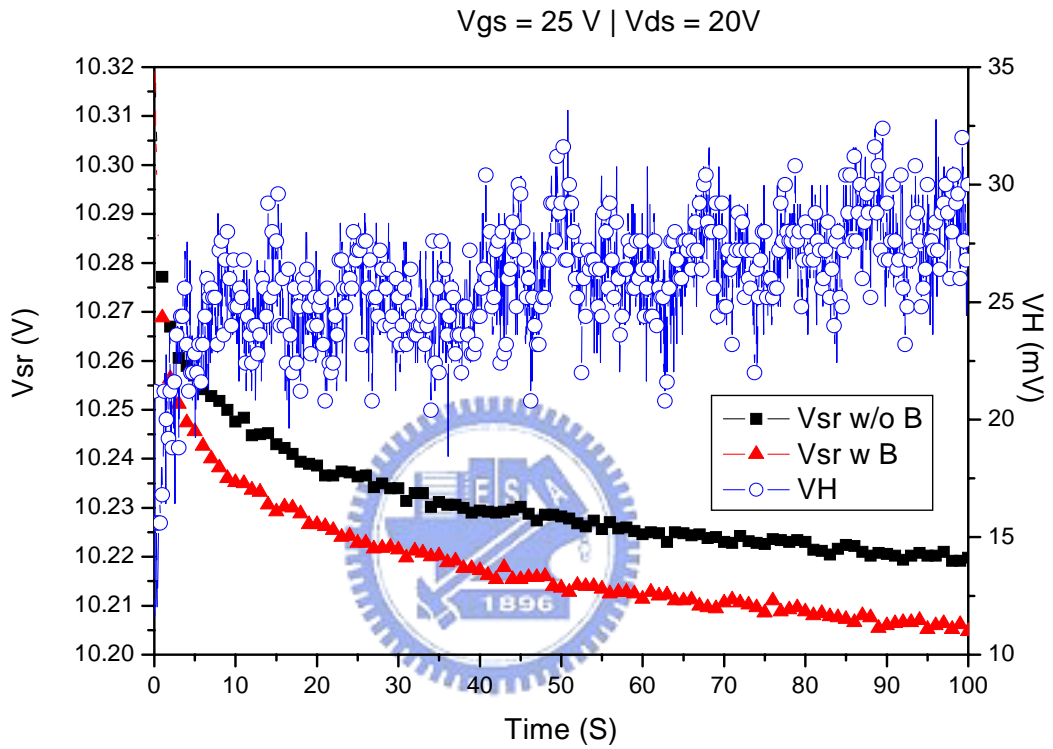


Fig. 4-11 The voltage of sensing electrode pad varies with time with/without magnetic field bias and Hall voltage versus time for $V_{gs} = 25 \text{ V}$, $V_{ds} = 20 \text{ V}$; $W/L = 40 \mu \text{ m}/100 \mu \text{ m}$; sensing pad is closed to source with the $20 \mu \text{ m}$

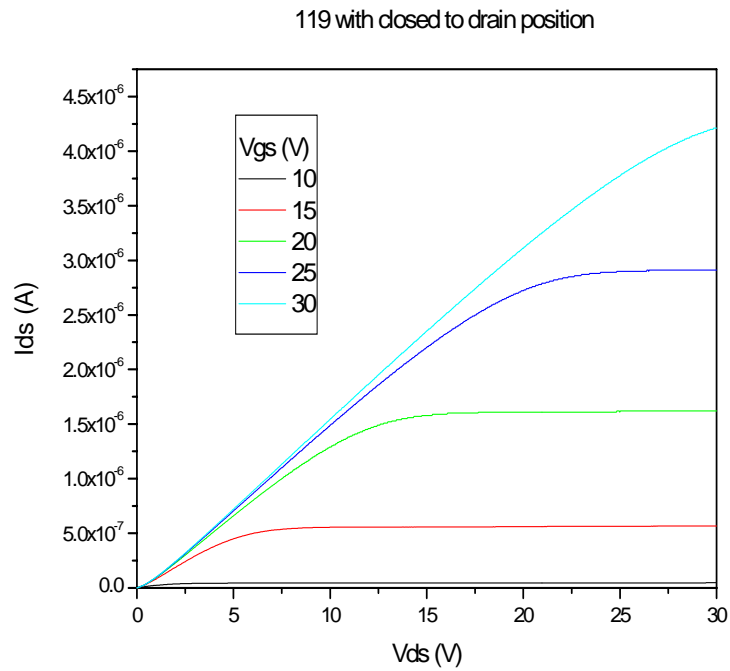


Fig. 4-12 Ids-Vds output characteristics of device 1 versus Vgs ; W/L = 40m/100m ; sensing pad is closed to drain with the 20m

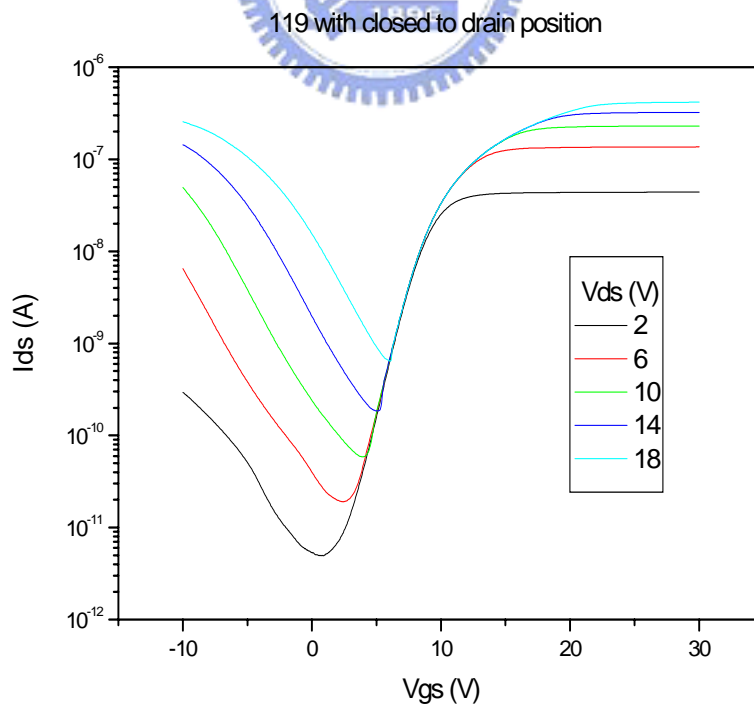


Fig. 4-13 Ids-Vds output characteristics of device3 versus Vgs ; W/L = 40m/100m ; sensing pad is closed to drain with the 20m

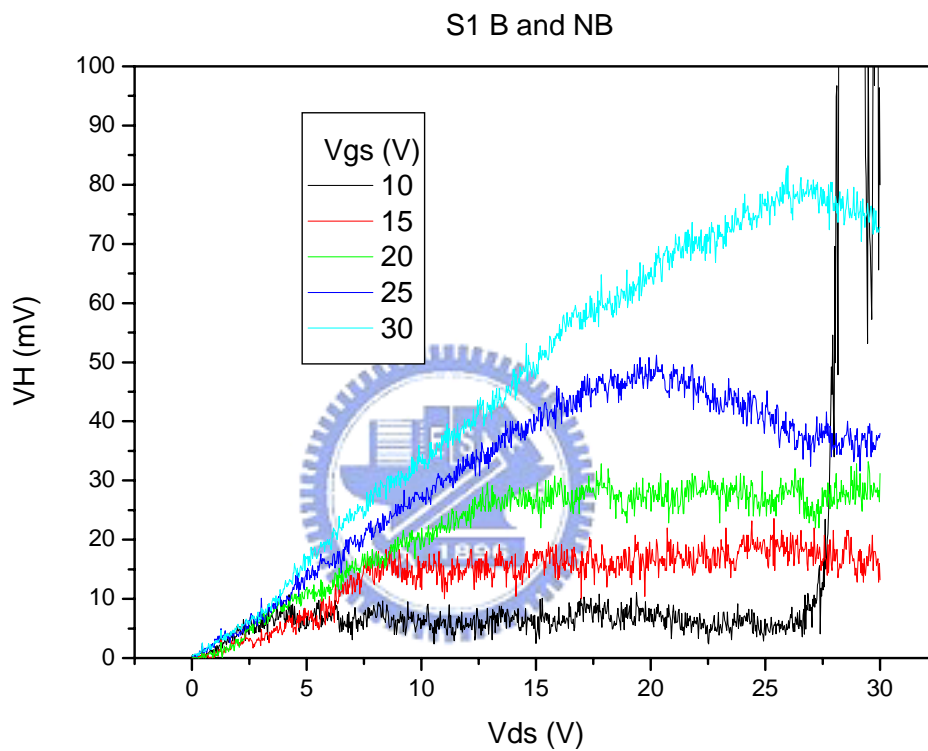


Fig. 4-14 Comparison of the Hall voltage versus V_{ds} for $V_{gs} = 10, 15, 20, 25, 30$ V ; $W/L = 40 \mu\text{m}/100 \mu\text{m}$; sensing pad is closed to drain with the $20 \mu\text{m}$; S1 is one of the sensing pads

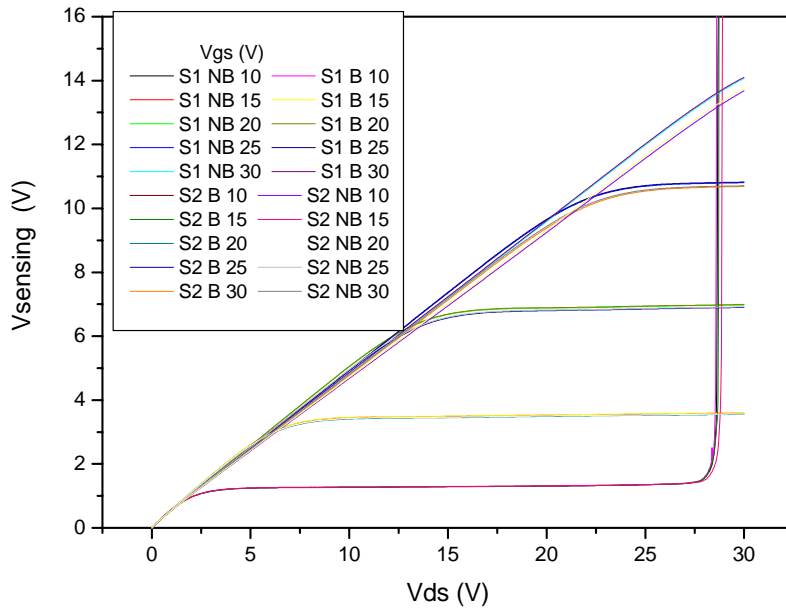


Fig. 4-15 The voltage difference of sensing electrode pad varies with time with/without magnetic field bias and Hall voltage versus V_{ds} for $V_{gs} = 10, 15, 20, 25, 30$ V ; $W/L = 40 \mu\text{m}/100 \mu\text{m}$; sensing pad is closed to drain with the $20 \mu\text{m}$

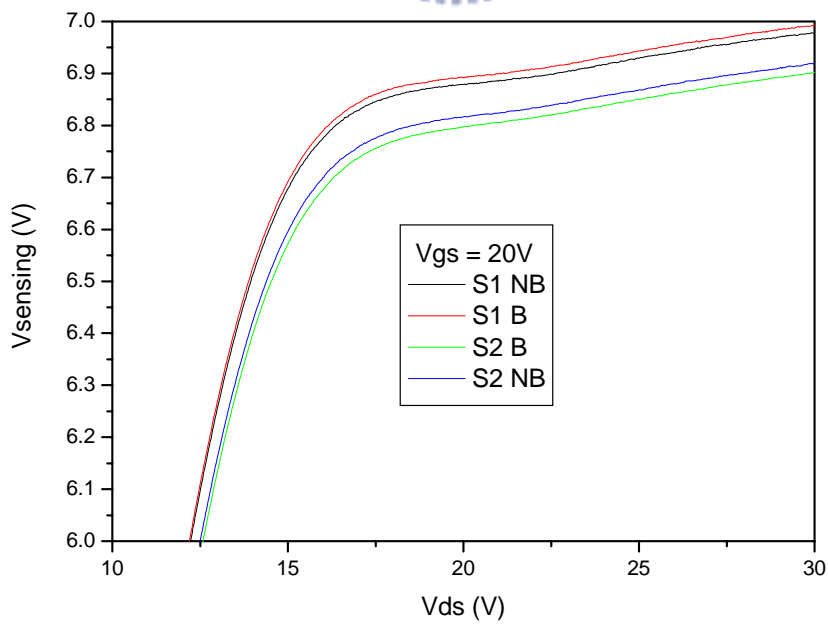


Fig. 4-16 The partial region of the Fig. 4-16

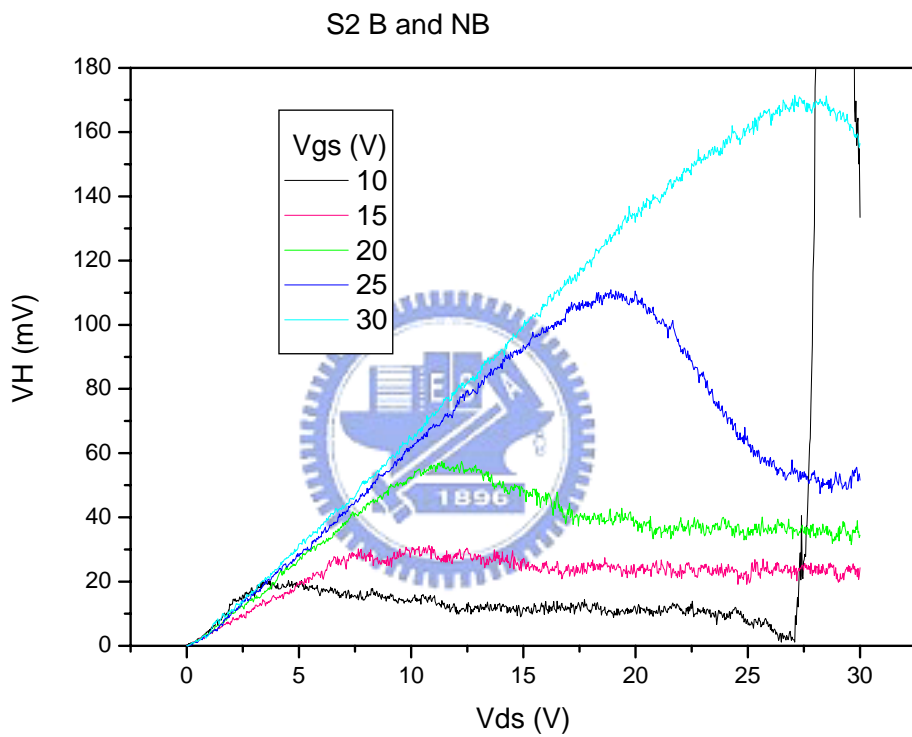


Fig. 4-17 Comparison of the Hall voltage versus Vds for Vgs = 10,15,20,25,30 V ; W/L = 40 μ m/100 μ m ; sensing pad is closed to drain with the 20 μ m ; S2 is another pad

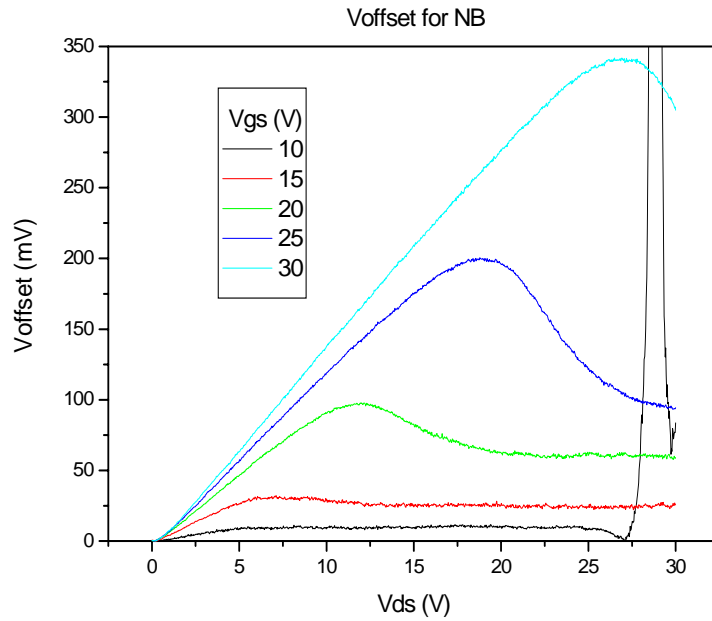


Fig. 4-18 Comparison of the offset voltage versus Vds for Vgs = 10,15,20,25,30 V ; W/L = 40 μ m/100 μ m ; sensing pad is closed to drain with the 20 μ m

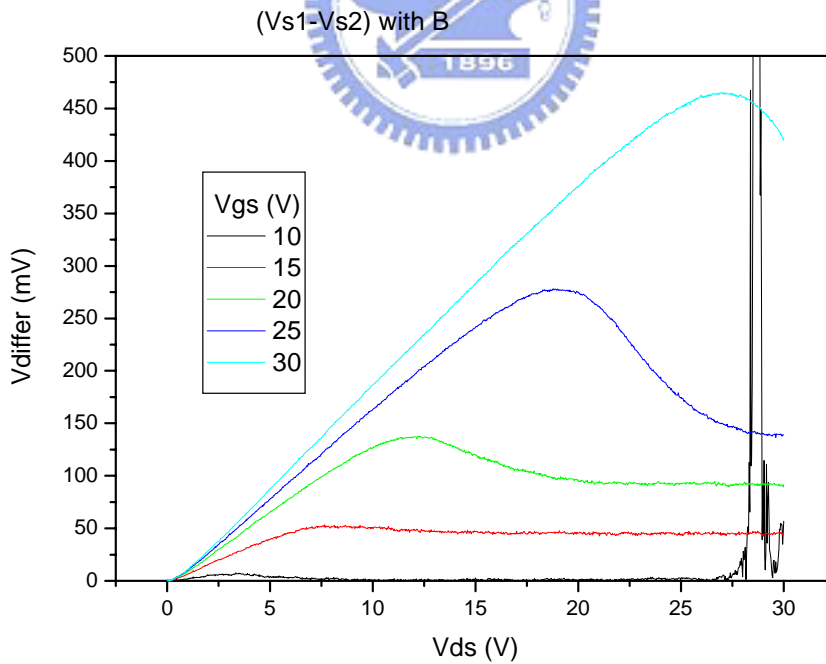


Fig. 4-19 The voltage gap between two pads with magnetic field versus Vds for Vgs = 10,15,20,25,30 V ; W/L = 40 μ m/100 μ m ; sensing pad is closed to drain with the 20 μ

簡歷

姓 名：蕭宇盛

性 別：男

出生日期：民國 69 年 03 月 16 日

出 生 地：台灣省嘉義縣

住 址：高雄市苓雅區福德二路 75 巷 1 號

學 歷：國立成功大學水利系（民國 87 年 9 月~92 年 6 月）

國立交通大學電子工程所碩士班（民國 92 年 9 月~94 年 6 月）

碩士論文：薄膜電晶體磁場感測器之研究

A study of Hall effect magnetic sensors based on polysilicon TFTs

